HHS Public Access

Author manuscript

Glia. Author manuscript; available in PMC 2017 May 01.

Published in final edited form as:

Glia. 2016 May ; 64(5): 668–694. doi:10.1002/glia.22953.

Traumatically injured astrocytes release a proteomic signature modulated by STAT3 dependent cell survival

Jaclynn Levine[1], **Eunice Kwon**[1], **Pablo Paez**[2], **Weihong Yan**[3], **Gregg Czerwieniec**[3], **Joseph A. Loo**[3,4,5], **Michael V. Sofroniew**[6], and **Ina-Beate Wanner**[1]

[1]Semel Institute for Neuroscience and Human Behavior, David Geffen School of Medicine, University of California Los Angeles, Los Angeles, CA, 90095-1763, USA

[2]Hunter James Kelly Research Institute, Department of Pharmacology and Toxicology, School of Medicine and Biomedical Sciences, SUNY, University at Buffalo, NYS Center of Excellence, Buffalo, NY 14203, USA

[3]Department of Chemistry and Biochemistry, University of California Los Angeles, Los Angeles, CA, 90095, USA

[4]Department of Biological Chemistry, David Geffen School of Medicine, University of California, Los Angeles, CA, 90095, USA

[5]UCLA/DOE Institute for Genomics and Proteomics, University of California, Los Angeles, CA, 90095, USA

[6]Department of Neurobiology, David Geffen School of Medicine, University of California Los Angeles, Los Angeles, CA, 90095-1763, USA

Abstract

Molecular markers associated with CNS injury are of diagnostic interest. Mechanical trauma generates cellular deformation associated with membrane permeability with unknown molecular consequences. We used an *in vitro* model of stretch-injury and proteomic analyses to determine protein changes in murine astrocytes and their surrounding fluids. Abrupt pressure-pulse stretching resulted in the rapid release of 59 astrocytic proteins with profiles reflecting cell injury and cell death, i.e. mechanoporation and cell lysis. This acute trauma-release proteome was overrepresented with metabolic proteins compared to the uninjured cellular proteome, bearing relevance for post-traumatic metabolic depression. Astrocyte-specific deletion of signal transducer and activator of transcription 3 (STAT3-CKO) resulted in reduced stretch-injury tolerance, elevated necrosis and increased protein release. Consistent with more lysed cells, more protein complexes, nuclear and transport proteins were released from STAT3-CKO versus non-transgenic astrocytes. STAT3-CKO astrocytes had reduced basal expression of GFAP, lactate dehydrogenase B (LDHB), aldolase C (ALDOC) and astrocytic phosphoprotein 15 (PEA15), and elevated levels

Corresponding author: Ina B. Wanner, PhD, Semel Institute for Neuroscience and Human Behavior, 635 Charles E Young Drive South, NRB 260, UCLA, Los Angeles, CA 90095. iwanner@mednet.ucla.edu.

The authors have no financial conflicts or interests.

Author contributions: IBW designed the research with contributions from MVS, PP and JAL. IBW, JL, EK as well as students and assistants acknowledged below performed experiments. IBW, JL, EK and WY analyzed the data with advice from PP, JAL, MVS and statistical input by Jeff Gornbein, PhD (see acknowledgment). IBW, JL, MVS and JAL wrote and edited the paper.

of tropomyosin (TPM4) and α actinin 4 (ACTN4). Stretching caused STAT3 dependent cellular depletion of PEA15 and GFAP, and its filament disassembly in subpopulations of injured astrocytes. PEA15 and ALDOC signals were low in injured astrocytes acutely after mouse spinal cord crush injury and robustly expressed in reactive astrocytes one day post-injury. In contrast, α crystallin (CRYAB) was present in acutely injured astrocytes, and absent from uninjured and reactive astrocytes, demonstrating novel marker differences among post-injury astrocytes. These findings reveal a proteomic signature of traumatically-injured astrocytes reflecting STAT3-dependent cellular survival with potential diagnostic value.

INTRODUCTION

After trauma to the CNS, mechanical impact from a pressure wave or physical deformation force acutely inflicts cellular injuries to neurons, glia and endothelial cells. This primary trauma impact causes acute plasmalemmal permeability, mechanoporation, resulting in "membrane deformation or failure" (Barbee 2005) that is demonstrated by cellular dye uptake acutely after injuries to the brain or spine (Choo et al. 2007; Farkas et al. 2006; Whalen et al. 2008). Diffuse axonal injury is a well-recognized pathophysiology due to neuronal membrane damage (Buki and Povlishock 2006). Acute astrocyte injury and demise after trauma are reported, but these early events in glia are poorly understood and have been overshadowed by studies examining delayed reactive astrogliosis (Colombo et al. 1997; Li et al. 2012; Sofroniew and Vinters 2010; Zhao et al. 2003).

Changes in protein composition of cells after mechanical trauma inflicting membrane integrity compromise are not known. Despite proteomic studies and advances in high fidelity neurotrauma models (Kwon et al. 2011; Lubieniecka et al. 2011), insight into cellular and molecular pathophysiology early after mechanical injury remains elusive. Analyses are confounded by diverse responses including trauma-inflicted cell damage, cell death, proliferation, inflammation and reactivity that occur over various times in different cell types (Burda and Sofroniew 2014). Changing cell composition due to infiltrating cells prevents standardized tissue sampling, making it difficult to isolate cellular and molecular injury mechanisms (Kazanis 2005; Shen et al. 2014; Wanner et al. 2013). Further, tissue homogenization mixes cells, interstitial fluids and blood, precluding the measurement of protein shifts between cellular and extracellular compartments. Our rationale is to identify protein changes specific to acute cellular traumatic injury and to determine an astroglial signature of traumatic protein release into surrounding fluids. We have chosen a simple, well-characterized and controlled *in vitro* injury model that produces widespread and reproducible mechanical strain injury to cells grown on deformable membranes by abrupt pressure-pulse stretching producing traumatic deformation forces (Wanner 2012; Wanner et al. 2008; Ellis et al. 1995; Shreiber et al. 1999).

In this study, we determined the changes in protein composition in astrocytes and their surrounding fluids acutely after mechanical trauma (Sondej et al. 2011). The resulting protein release profiles of traumatized mouse astrocytes were related to inflicted transient mechanoporation, cell injury, or cell death. Mice with astrocyte-selective deletion of STAT3 were used to capture acute trauma-induced differences in astrocyte injury responses

dependent on an acute survival role of STAT3 in traumatized astrocytes. While STAT3 activation has been shown to govern reactive gliosis after spinal cord injury (Herrmann et al. 2008; Wanner et al. 2013), we focus on its acute role in astroglial survival after traumatic injury. Our studies using genetic deletion and acute pharmacological inhibition of STAT3 show its critical role in survival of acutely traumatized astrocytes, and we identify various new STAT3-regulated astrocytic proteins.

This work provides the first fluid-derived proteomic signature of traumatized astrocytes, the mouse astrocyte trauma-release proteome. Trauma-released proteins reflect the extent of mechanoporation and cell death. Cell population fate analyses document cytosolic protein depletion, induction and posttranslational modification after mechanical trauma in injured and reactive astrocytes. This study is translationally significant because it provides a fluid-based astrocyte signature of trauma that carries potential diagnostic marker candidates.

MATERIALS AND METHODS

Animals

All mice used were derived from in-house breeding colonies backcrossed onto C57/BL6 backgrounds. Mice with astrocytic STAT3 (conditional knockout, STAT3-CKO) were generated by mice having loxP sites flanking the exon 22 of the STAT3 gene, encoding a tyrosine residue (Y705) essential for STAT3 activation (Takeda et al. 1998). STAT3 loxP mice were crossed with the mGFAP-Cre mouse line 73.12. We characterized the resulting mGFAP-STAT3-CKO mice in the context of SCI (Herrmann et al. 2008; Wanner et al. 2013). Control mice (CON) included (i) no transgene, (ii) were heterozygous for mGFAP-Cre, or (iii) were heterozygous or homozygous for loxP without carrying mGFAP-Cre (Herrmann et al. 2008). All experiments were approved by the Animal Research Committee of the Office for Protection of Research Subjects at UCLA. Mice were genotyped by PCR (Hermann et al., 2008) and Western blotting.

Moderate mouse spinal cord crush injury surgical procedure

All surgical procedures were performed under general anesthesia with isoflurane in oxygen-enriched air using an operating microscope (Zeiss), and rodent stereotaxic apparatus (David Kopf). Crush injury was made after laminectomy of a single vertebra at the level of L1/L2 using No. 5 forceps (Dumont, Fine Science Tools, tip width of 0.5 mm, fitted with a 0.25 mm spacer) compressing the cord for 5 seconds (Faulkner et al. 2004). This inflicted a moderate crush injury for CON mice but exacerbated severity for STAT3-CKO mice (Herrmann et al. 2008). Animals were evaluated blind to genotype and experimental condition. Spinal cords were analyzed 6 hours (h), 1 day (D) and 3 D post-injury.

Astrocyte cell culture and in vitro trauma

Cortical tissue from 3–4 D old mice was dissected, cut into < 0.5 mm pieces in cold Ca^{2+} and Mg^{2+}-free HBSS (Wanner 2012). Cells were isolated by trituation in medium (DMEM/F12, 10% FBS, 1:1000 gentamicin), filtered through nylon meshes (70 μm, then 10 μm) and collected by centrifuging (6 min at 380 x g). Cells of each animal were resuspended and

cultured in individual T25 flask in same medium. Upon reaching confluence, proliferating cells were removed by shaking (de Vellis et al. 2009).

Astrocytes were passaged onto deformable membranes after a brief Versene rinse (137 mM NaCl, 1.5 mM KH_2PO_4, 2.7 mM KCl, 8.1 mM Na_2HPO_4, 685 μM EDTA) followed by 6 min digestion with 0.25% trypsin in 0.53 mM EDTA at 37°C that was stopped by adding medium and centrifugation at 400 x g. After resuspension in the same medium, 150–200,000 cortical cells per 2.5 ml medium were seeded onto each elastic culture well (962 mm^2). Upon confluence medium with heat inactivated 10% adult horse serum was used, which was stepwise withdrawn. Cultures were serum free prior to stretching and contained postmitotic cells expressing mature markers (Wanner 2012; Wanner et al. 2008).

Cells were mechanically stretch-injured using a controlled pneumatic pressure device (2^{nd} generation cell injury controller, CIC II, Custom Design and Fabrication Inc.). A 50 ms nitrogen pressure-pulse deformed the elastic culture bottom, causing widespread astrocyte stretching and shearing. Injury pressures between 2.1–2.7 psi lead to 11.2–12.2 mm deflection of the BioFlex II plates using the CIC II (CIC Operation Manual). Cells and media were analyzed at 5, 30 min, at 5 and 48 h post-injury.

Time-lapse imaging, membrane permeability and cell death analysis

Astrocytes from 9 CON and 8 STAT3-CKO mice were monitored on a time-lapse microscopy stage. In addition, 5 CON cultures were pretreated overnight with the STAT3 inhibitor indirubin, 10 μM E804, which was removed prior to imaging (IRE, Nam et al. 2005). Plasmamembrane permeability was assayed using 10 kD dextrans conjugated with fluoro-rhodamine or Alexa Fluor 555 that was (0.05 mM, Molecular Probes) replaced 3 min post-stretching. A 25 mm diameter circle was cut out of the silastic culture bottom using a leather puncher (arch puncher) and was placed upside down into a 35 mm glass bottom culture dish with a recessed space (Matek Corp.) fixed by a messing ring. Pre-warmed Alexa 488 conjugated caspase 3 substrate was added (10 μM, NucView 488 caspase 3 substrate, Biotium). Within 15 min the dish was transferred onto a stage top chamber with 5% CO_2 at 37°C (Wheather station, Precision Control) and 6 areas per culture were monitored using a spinning disc confocal inverted microscope (Olympus IX81). Focus corrected images were obtained at 6 min intervals, using a 10X phase contrast objective (UPlan FLN, numerical aperture, NA 0.3) with appropriate filters for red (excitation λ: 535–555 nm, emission λ: 570–625 nm) and green (excitation λ: 457–487 nm, emission λ: 502–538 nm) and a CCD camera (ORCA-R2, Hamamatsu). Images were analyzed between 30 min, as caspase substrate conversion became visible and 4.5 h after stretching (SlideBookTM 4.1, Intelligent Imaging Innovations). Intact and dead cells were determined on phase-contrast images by counting nuclei of unlysed (gray) and lysed cells (phase-dark nuclei with white halo). Permeable, resealed injured cells were determined by counting fluoro-rhodamine-dextran positive cells. Apoptotic cells were determined by counting Alexa 488 caspase substrate positive nuclei. Cell fractions were determined from 7 stretched cultures of CON mice, 6 STAT3-CKO mice and 5 IRE treated cultures and normalized to their respective genotype unstretched cultures (n=5).

A 10 min propidium iodide (PI, 60 μM in pre-warmed Leibovitz' medium, Sigma) uptake in unfixed cells determined percentages of cell death and permeability (molecular weight: 668 Da) at 5, 30 min or 48 h after stretching. PI stain was crosslinked by UV light for 5 min after rinses in same medium. Cultures were fixed for 30 min in cold, freshly depolymerized 4% PFA in TBS (pH 7.4, filtered).

Proteomic analysis: sample preparation, and 2-D gel electrophoresis

A detailed proteomic protein preparation protocol is provided (Sondej et al. 2011). Conditioned medium (CM, "fluid", 24 ml, 12 cultures per condition) at 30 min and 5 h after injury was supplemented with DTT (5 mM) and protease inhibitors (Roche, 2.5 tablets/24 ml, including 1 mM EDTA). Debris was removed by centrifuging media for 5 min at 600 x g (J-6B, Beckman). Fluid samples were concentrated to one twentieth of the volume (3 kD molecular weight cutoff centrifugal concentrators, Vivaspin, GE Healthcare), yielding a final protein amount between 1–1.6 mg. Samples were desalted using Sephadex G-25 desalting columns (PD10 spin columns, GE Healthcare) and proteins were precipitated in cold 10% TCA and then centrifuged for 10 min at 17,400 x g (RC-5C Plus, Sorvall). Pellets were rinsed in H_2O followed by 10x volume of cold acetone, and stored overnight at −20°C. Samples were centrifuged (10 min, 17,400 x g, 4°C), supernatants removed and pellets were air dried. Proteins were resuspended in 500–900 μl rehydration solution (7 M urea, 2 M thiourea, 4% CHAPS, 0.2% Bio-Lytes pH 3–10, 0.0002% bromophenol blue and 0.4% DTT) and the protein concentration was assayed using a colorimetric assay read at 660 nm (Pierce).

For the first dimension isoelectric focusing gel electrophoresis, samples were centrifuged for 5 min at 16,000 x g, 4 °C, diluted to 0.5 μg protein/μl rehydration solution and 200 μl (100 μg) was loaded onto each of triplicate immobilized pH gradient (IPG) strips (11cm, pH 3–11 nonlinear ReadyStrip, Biorad). After incubating for 1 h at room temperature (RT), strips were overlaid with mineral oil and actively rehydrated overnight at 50 V, 20 °C in an isoelectric focusing cell (Protean). Isoelectric focusing proceeded by applying a maximum current of 30 μA/strip using 4 h at 100 V (linear) followed by 2 h at 250 V (linear), 5 h at 4,000 V (linear) and then for 85,000 volt-h at 4,000 V (rapid) at 20 °C.

For the second dimension, the proteins in the IPG strips were reduced using 2% DTT in 50 mM Tris-HCl (pH 8.8), 7 M urea, 20% glycerol, 2% SDS for 20 min with gentle shaking at RT and then alkylated using 2.5% iodacetamide in the same buffer. IPG strips were placed on top of precast 10.5–14% gradient SDS-PAGE gels (Criterion, Biorad), overlaid with pre-warmed low melting agarose (0.5%, 0.008% bromophenol blue in 1X SDS-PAGE running buffer), and run at 19 °C starting for 10 min at 40 V, followed by 2–2.5 h at 120 V in 25 mM Tris (pH 8.3), 192 mM glycine, 0.1% SDS along with unstained molecular weight standards (Benchmark, Invitrogen, Dodeca Criterion, Biorad). Gels were rinsed in water, fixed for 1 h in fixer solution (10% methanol, 7% acetic acid) and stained overnight at RT with Sypro Ruby (Biorad). Gels were rinsed, destained for 4 h in fixer solution and fluorescence was scanned (532 nm excitation, 555 nm LP emission filter; FX Pro Plus, Biorad).

Matching spot intensities were quantified in unstretched and stretched samples using triplicate gels per condition (SameSpots software, Progenesis). Cultures from 11 CON mice and 8 STAT3-CKO mice were analyzed. Stretched cultures of 6 CON and 4 STAT3-CKO mice were compared with unstretched cultures (5 CON, 4 STAT3-CKO) in triplicate for each sample. Spot changes with at least 1.8-fold difference and a probability of $P<0.05$ were defined as significant (multiple comparison ANOVA). Proteins with levels unchanged by stretching were also found (Fig. 2 A_1).

Mass spectrometry for gel spot identification and mouse astrocyte proteomes

Selected spots were excised from the 2D gels using a robotic spot cutter (ProPic II, Digilab). Proteins were trypsin digested (Shevchenko et al. 1996), peptides extracted and vacuum concentrated (SpeedVac, Thermo). Peptides were reconstituted with 20 μl of 2% acetonitrile, 0.1% formic acid and 10 μl (≈100–200 fmol peptides) were loaded on a C18 Nano-Trap pre-column (Dionex) using a flow rate of 5 μl/min. Peptides were separated by a C18 analytical HPLC column at a flow rate of 300 nl/min with an increasing acetonitrile gradient. Peptides were measured by LC-tandem mass spectrometry (LC-MS/MS) using a hybrid linear ion trap mass spectrometer (LTQ-Orbitrap) with a pico/silica tip ESI emitter (New Objective) and helium as collision gas. Data dependent non-redundant MS/MS spectra were acquired using: R = 100,000; full range *m/z* 300–2000 scan followed by 7 MS/MS scans for most intense peptide ions. Sequences of mass spectra were searched (Mascot, Matrix Science) and identified (Swiss-Prot mouse database). Criteria for protein identification for a greater than 95% confidence required a minimum of two unique peptides with an ion score greater than 34 and were manually validated.

LC-MS/MS was used to determine the proteome of mouse astrocytes and their released proteins. Unstretched astrocytes were grown in T75 flasks. Medium (11 ml/flask) was collected supplemented with EDTA (5 mM), bestatin (40 μM), pepstatin (10 μM) and phosphoramidon (10 μM), concentrated and desalted. Cells were lifted by shaking in Versene pelleted (centrifugation for 5 min at 100 x g), and then lysed in 0.5% NP40, 150 mM NaCl, 25 mM Tris, including same protease inhibitor additives. Upon homogenization with a G25 then G27½ needle, whole cell lysates (WCL) were diluted to 0.1% NP40. Part of the samples was depleted from abundant proteins using either immunoaffinity (Sigma ProteoPrep) or silicon carbide ion exchange based enrichment (Norgen ProteoSpin). Protein concentration was determined and samples were vacuum-concentrated and adjusted to pH 8 using freshly prepared 100 mM NH_4HCO_3 buffer. Proteins were reduced in the same buffer with 5 mM DTT for 20 min at 50°C followed by 5 min at 96°C, and then alkylated with 10 mM iodacetamide in 100 mM NH_4HCO_3 for 45 min at 37°C. Fluid samples of 10–50 μg protein per 50 μl medium and cell lysates of 20–90 μg protein per 100 μl WCL were trypsin digested overnight at 37°C using 1–2 μg trypsin. Digested protein (1.0–1.5 μg) was loaded on the C18 Nano-Trap pre-column at 5 μl/min for 5 min and separated by a C18 HPLC column at a flow rate of 300 nl/min with an increasing acetonitrile gradient. Peptides were measured by LC-MS/MS using the same instrument (LTQ-Orbitrap).

Western blotting and statistical analyses

Fluid (CM) proteins were prepared as described omitting desalting and precipitation. WCL proteins were prepared by adding 150 μl/well of ice cold lysis buffer (150 mM NaCl, 20 mM Tris, 5 mM EDTA, 10 mM sodium pyrophosphate, 30 mM phosphatase substrate, 5 mM DTT, 1% NP40 and 1 protease inhibitor tablet per 10 ml buffer). Cells were collected and homogenized by trituation, passaged through a 27½ gauge needle avoiding bubbles, and protein concentration was determined.

One fifth of Laemmli sample buffer (6x) was added to samples (125 mM Tris-HCl, pH 6.8, 10% glycerol, 2% (w/v) SDS, 0.1% (w/v) bromophenol blue), samples were denatured by boiling for 5 min at 100°C, and placed on ice. Protein (30 μg) was loaded on 10% or 15% Tris-HCl polyacrylamide handcast gels (Mini-PROTEAN, Bio-Rad) along with a molecular weight standard (Precision Plus Protein™ Kaleidoscope, Bio-Rad). Gels were run in SDS running buffer (200 mM glycine, 25 mM Tris Base, 0.1% (w/v) SDS) and blotted onto nitrocellulose membranes (Amersham Hybond-ECL, GE Healthcare) in 200 mM Glycine, 25 mM Tris (pH 8.3), 20% methanol. Blots were stained for 10 min with 0.1% Ponceau S in 5% acetic acid and gels were stained overnight at 4°C using 0.4% Brilliant Blue R, 45% methanol, 10% acetic acid. Membranes were washed with Tween (0.05%) supplemented Tris buffered saline (TBST) and incubated in 10% dry milk in TBST for 1 h at RT. Washed blots were incubated in primary antibody diluted in 5% BSA in TBST overnight at 4°C (Table 1). After rinsing, blots were incubated for 1 h at RT in secondary antibodies coupled to horseradish peroxidase diluted in 10% milk in TBST (Table 2). Proteins were visualized using enhanced chemiluminescent substrate (Supersignal West Pico, or Femto; Thermo Scientific) and autoradiography film (Hyblot CL, Denville Scientific).

Western blots of cultures from 11 CON and 9 STAT3-CKO animals were analyzed. A ranked intensity score was assigned to each of the 13 proteins (0, no signal; 4, maximal signal within a blot) of stretched and unstretched, CON and STAT3-CKO samples processed together. Protein *release* was implied when an intracellular protein, based on its gene ontology (GO) assignment, was elevated (≥0.5 difference from base level) in the fluid in at least 4 different animals on Western blots and was significantly increased on 2-D gels (Table 3). Statistical comparisons of injury and genotype mean intensity differences were made using a non-parametric repeated mixed measure ANOVA model and resampling, since ordinal intensity data did not follow the normal distribution (Efron and Tibshirani 1991). Means that followed the normal distribution were compared using t-tests or parametric one way ANOVA. Significance was assessed using the Tukey-Kramer criterion to adjust for multiple comparisons. Trauma-induced changes were compared to baseline. Differences between CON and STAT3-CKO astrocytes were determined in unstretched WCL samples from 5–8 genotype culture pairs. Injury differences between genotypes were compared in stretched CON and STAT3-CKO cultures correcting for variability due to different penetration of the STAT3 deletion. Spearman's correlations were computed between protein release amounts and cell death. Factor analysis based on Spearman correlations determined commonality among multiple proteins based on genotype. Statistical analyses were carried out using SAS9.4 (SAS Inc.) and Instat (GraphPad Inc.).

Immunocytochemistry for PEA15 and GFAP as well as permeability and death analysis

After rinsing the cells, non-specific binding was blocked by 5% normal donkey serum (NDS). Rabbit anti-PEA15 and chicken anti-GFAP were applied overnight in blocking solution at 4 °C (Table 1). Donkey anti-rabbit Alexa Fluor 488 and anti-chicken Alexa Fluor 647 were diluted in the same blocking solution and centrifuged for 30 min at 13,000 x g, 4 °C and incubated for 1 h in the dark at RT on rinsed cultures (Table 2). After rinsing, cultures were stained for 5 min with 10 μg/ml bisbenzimide in H_2O (Hoechst, Sigma), rinsed, dried and coverslipped using a 25 mm circular cover glass (491 mm^2) and solidifying anti-fade mounting medium (Fluoro-gel, Electron Microscopy Sciences). Dried membranes were cut and mounted onto glass slides with 8% gelatin solution. Slides were fitted with tape strips (3M) for imaging on an inverted fluorescence microscope (Olympus IX70) equipped with a CCD camera and capturing program (Axiocam, Axiovision, Zeiss).

Cultures from 4–6 CON and 3–4 STAT3-CKO animals for each condition (unstretched, 5, 30 min and 48 h post-stretching) were stained. Twelve pictures per culture were analyzed using a 20x objective (UPLAN Apo, NA 0.7, PH2) and 600 to 1140 cells per culture were scored for incidences of PI-, PEA15- and GFAP-positive cells. GFAP cytoskeletal filament assembly, brightness subcellular localization were scored. Filament disassembled GFAP signals appeared homogeneous and blurred adjacent to filament assembled GFAP displaying typical cytoskeletal lines, supporting a structural change in selected cells after stretching. The proportion of PI-positive cells among the PEA15 and the various GFAP populations was determined. Astrocytes with granular GFAP were excluded. “Intact cells” were PI-negative with oval nuclei with pale Hoechst staining. “Dead cells” had shrunken, pyknotic, raisin-shaped nuclei with condensed, bright Hoechst-stained nuclei. The “acute” post-injury dataset combined 5 and 30 min post-stretching. Significant differences in numbers of PEA15- and GFAP-positive cell populations and PI-positive cells among them were determined using post-hoc multiple comparison ANOVA (Tukey, Instat).

Spinal cord immunohistochemistry and image analysis

After terminal anesthesia by barbiturate overdose, mice were perfused transcardially with buffered 4% PFA. Spinal cords were removed, post-fixed for 2 h and cryoprotected in buffered 30% sucrose overnight. Horizontal, 40 μm frozen sections were cut using a cryostat microtome (Leica).

For enzyme-enhanced immunohistochemistry, endogenous peroxidase was quenched for 15 min using 1% H_2O_2 in 100% methanol, then sections were permeabilized for 45 min in 0.5% Triton X100, rinsed and incubated in 5% normal goat serum in TBS. Rabbit anti-aquaporin 4 and rabbit anti-GFAP were combined in the same blocking solution and incubated overnight at 4 °C (Table 1). After rinsing, biotinylated anti-rabbit antibody was incubated in blocking solution for 1 h at RT (Table 2). After incubation and rinsing an avidin-biotin-peroxidase complex (ABC kit, Vector) was prepared and applied to the sections. Rinsed sections were equilibrated in 100 mM sodium acetate buffer and the freshly prepared, sonicated and filtered modified DAB substrate solution (0.5 mg DAB/ml, 2 mg β-D-glucose /ml, 6 units glucose oxidase /ml and 25 mg nickel ammonium sulfate /ml in 100 mM sodium acetate buffer) was applied at RT for 5–10 min and stopped by rinses in acetate

buffer (Shu et al. 1988). Sections were rinsed, thaw-mounted onto glass slides in 0.5% gelatin solution, dried and dehydrated in an increasing ethanol series, rinsed in xylene and mounted (Permount) with weights for 20 min at 70 °C on a slide warmer. DAB-stained sections were photographed on an upright brightfield microscope (AX70, Olympus) and images of various focus levels were overlaid in Photoshop (Adobe).

For immunofluorescence (IF) staining endogenous tissue autofluorescence was blocked by incubating water-equilibrated sections in a 0.5% Sudan black solution in 70% ethanol for 5 min followed by rinses. Sections were permeabilized in 0.5% Triton X100 in TBS for 20 min, rinsed and incubated for 2–4 h in 5% NDS in TBS. Goat anti-ALDOC and mouse-anti-CRYAB were each combined with rabbit anti-GFAP. Rabbit anti-PEA15 was combined with chicken anti-GFAP in 5% NDS in TBS and sections were incubated overnight at 4 °C. After rinsing, anti-goat Alexa 488 combined with anti-rabbit-Cy3, anti-mouse Cy3 combined with anti-rabbit Alexa 488 and anti-rabbit-Alexa 488 combined with anti-chicken Cy3 were prepared in blocking solution, centrifuged for 30 min at 13,000 x g at 4 °C and incubated on the sections for 1 h at RT (Table 2). Rinsed sections were stained for 5 min with 10 μg/ml bisbenzimide in H_2O. After final rinses, sections were dried and coverslipped as above. Sections were analyzed using a confocal laser scanning microscope (LSM 510, Zeiss) with a 63x oil immersion objective (PLAN Apochromat, NA 1.4), a 488 nm argon laser and a 543 nm helium-neon laser with a 505–530 nm bandpass filter for Alexa 488 fluorescence, and a 560–615 nm bandpass filter for Cy3 fluorescence. The same pinhole (1 μm) and photomultiplier settings were used for all images and scans over a depth of 4 μm were overlaid.

RESULTS

Acute STAT3 activation is important for cell integrity and apoptosis after astrocyte injury

Cell death rates rose with increasing pressure intensities 48 h post-injury with exacerbated dose-response relationship in STAT3 deficient astrocytes (STAT3-CKO) compared to controls (CONs, Fig. 1A). Stretch pressures of 2.4 ± 0.3 psi caused cell death in one fifth of stretched CON and nearly half of STAT3-CKO astrocytes, a 2.4 fold difference (Fig. 1B). Post-injury membrane permeability was monitored by a 10 kDa rhodamine-conjugated dextran and apoptosis using a green fluorescent caspase 3 substrate. Time-lapse video analysis shows that 22% of astrocytes stained with rhodamine-dextran during stretching retained the dye following washing (Fig. 1C). These “resealed injured” astrocytes were membrane porated during stretching and regained cell integrity afterwards, which is a new finding. Acute cell lysis occurred in 23% of CON astrocytes, without significant additional subsequent necrosis, while rates were higher in STAT3-CKO astrocytes, and necrosis continued over time post-injury (Fig. 1D). Apoptotic CON cells rose from 10% at 30 min to 25% by 4.5 h post-injury (Fig. 1D), with some resealed injured cells becoming apoptotic (Fig. $1C_4$). There were hardly any apoptotic cells among STAT3-CKO stretched astrocytes anytime post-injury (Fig. $1C_8$, 1D). Most leaky STAT3-CKO astrocytes underwent lysis without activating caspase 3 by 4.5 h post-injury (Fig. 1D). Thus, abrupt pressure-stretching caused transient membrane permeability followed by apoptosis and necrosis that was

elevated in STAT3-deficient astrocytes, showing reduced survival and apoptosis; hence they were less stretch-resilient than controls.

We next tested whether STAT3-CKO astrocytes were more vulnerable due to a pre-existing deficiency of STAT3 regulated proteins (Sriram et al. 2004). We inhibited STAT3 prior to stretch-injury in non-transgenic astrocytes using the indirubin derivative E804 (IRE) that inhibits STAT3 activation without being toxic (Nam et al. 2005). All astrocytes had initially similar membrane permeability rates after stretching, yet dye-retaining rates were poor in IRE-treated (not shown) and STAT3-CKO astrocytes compared to controls by 4.5 h post-injury. IRE reduced apoptosis by 22% after stretching compared to untreated CON astrocytes (at 4.5 h, SEM is 6 in CON, 1 in IRE treated cultures, n=5 cultures, $P<0.01$, Tukey ANOVA). Stretch-induced necrosis rates of IRE-treated were similar to those of STAT3-CKO astrocytes and significantly higher than those of untreated CON astrocytes (by 23%, at 4.5 h, SEM is 2 in CON, 4 in IRE treated cultures; $P<0.01$, Tukey, ANOVA). Thus, we show for the first time that both, pharmacological inhibition and genetic deletion of STAT3 elevated necrotic cell death and suppressed apoptosis, making astrocytes without STAT3 activation more vulnerable to mechanical trauma and unable to overcome integrity compromise.

Identifying a mouse astrocyte trauma-release proteome

We next determined the release profile of traumatized astrocytes using a proteomic approach chosen for its robust and unbiased detection of protein differences. We reproducibly measured ~ 700 protein spots derived from fluid, i.e., conditioned medium (CM) from unstretched and stretched cultures of both genotypes at 30 min and 5 h post-injury. Spots with reproducibly different intensities (≥ 1.8x increase or ≤ 0.6x decrease) after stretching in either genotype were selected, excised and digested. We identified 59 trauma-influenced proteins by mass spectrometry (Fig. 2A), 53 proteins increased in CM (Fig. $2A_2$; Table 3) while 6 proteins decreased. Three change profiles were found at 30 min (Figure 2B) and similarly, at 5 hr after stretching (not shown). Example protein spots for each of these profiles with corresponding protein immunoblots confirmed the observed profiles (Figures 2C and D). 1: Similar stretch-induced protein increase in fluid of CON and STAT3-CKO cultures, as seen in Ywhae 14-3-3ε (1433E) and aldolase C (ALDOC, Fig. $2B_1$, C_1, D_1). 2: Larger protein increase in STAT3-CKO versus CON culture fluids post-injury, e.g. Cu-Zn superoxide dismutase 1 (SODC, Fig. $2B_2$, C_2, D_2). 3: Only CON fluids showed stretch-induced protein increase not -STAT3-CKO fluids, e.g. apolipoprotein E (APOE, Fig. $2B_3$, C_3, D_3). Thus, mechanical trauma caused acute and substantial release of astrocytic proteins with STAT3 modulated release profiles.

Gene ontology (GO) analysis shows that released proteins originated from all cellular compartments and across all functional categories (Fig. 3B, E). The largest group of released proteins was organelle-derived (37%), followed by cytoplasmic ones (23%, Fig. 3C for 30 min post-injury, 5hr data were similar, not shown). STAT3-CKO cultures had overall 1.7 fold more trauma-released proteins than CON cultures (Fig. 3A, 30 min post-injury, 5hr data were similar, not graphed, see Table 3). Proportionally more nuclear proteins and protein

complexes were released from STAT3-CKO versus CON stretched astrocytes, including filamin-A, an ATPase (OLA1) and β actin (ACTB, Fig. 3B).

To determine whether trauma caused selective or unselective protein release from the cellular pool, we identified all proteins of CON mouse astrocytes by proteomic mass spectrometry and (LC-MS/MS) compared their cellular compartments and functional assignments with that of trauma-released proteins (Fig. 3C, F). Trauma-released proteins originated from all subcellular compartments and fluids similarly (with the exception of membrane-bound organelles, which were nearly doubled (Fig. $3C_{1+2}$). This correlation was comparable for STAT3-CKO cells (not shown). Consistent with finding organelle-derived proteins, including peroxiredoxin 2, phosphatidyl ethanolamine binding protein (PEBP-1) and S-formylglutathione hydrolase/esterase D (ESTD), we frequently found dye-incorporated vesicles during lysis of membrane-permeable astrocytes after stretching Cytosolic dye uptake by membrane-wounded cells appeared in vesicles just prior to disappearing as cells lysed. (Fig. 3D). This reflects an organelle- mediated process, like vesicle-shedding, which was associated with trauma induced secondary cell death and might contribute to protein loss.

Extracellular space and plasma membrane proteins were common in CM of unstretched cultures (25% of the assignments, Greco et al. 2010), yet they were 2–3 fold under-represented in the trauma-release proteome (Fig. $3C_2$). Among these were classically secreted proteins, like APOE, gelsolin, haptoglobin, and inter-alpha-trypsin inhibitor that were decreased in fluids acutely after stretching (Fig. $2B_3$, C_3, D_3; Table 3). This finding suggests reduced active protein secretion as a new aspect of astroglial traumatic injury.

Considering astroglia's major roles in brain metabolism, inflammation and reactive gliosis, we analyzed the biological processes of the trauma-released proteins (Fig. 3E). Metabolic proteins were the largest acute trauma-release group of CON astrocytes after stretching at both times post-injury (Figs. 3E, F). Together with catabolic proteins, they contributed to one third of the trauma-release proteome. STAT3-CKO astrocytes had similar metabolic and catabolic proteins released. For example, GAPDH had the largest release amount from injured astrocytes in both genotypes (Table 3). Proteins of cell component organization, communication and transport were released more selectively by STAT3-CKO than CON injured astrocytes (Fig. 3E, shown are 30 min post-injury, 5hr had similar release profiles, not shown). Together, over-represented release of nuclear proteins and protein complexes from stretched STAT3-CKO astrocytes (Fig. 3B), suggests that cell lysis contributed more to the STAT3-CKO than to the CON release profile, which is consistent with finding elevated necrotic cell death in STAT3-CKO versus CON traumatized astrocytes (Fig. 1D).

We next compared biological processes of the trauma-released proteins with those of the cellular proteome of CON astrocytes (Fig. 3F). Again, most functional categories (9 out of 13) were released proportionally to their presence inside uninjured cells, except metabolic plus catabolic proteins, which were nearly doubled in the trauma-release proteome relative to their representation in cells. Release of metabolic proteins contained enzymes processing carbohydrates, such as aldolases, enolase, GAPDH, cytoplasmic isocitrate, malate dehydrogenases and LDHB. Amino acid processing enzymes like glutamine synthetase and

nitrogen compound related proteins including SODC, nucleoside diphosphate kinase B, and PEBP1 were also abundantly released. In contrast, proteins of cell communication, transport and cell component organization were underrepresented compared with the LC-MS/MS cell proteome (Fig. 3F, 30 min trauma-release profile, similar data at 5hr post-injury, not shown). Biological process assignment of STAT3-CKO released profiles was not compared to their whole cell lysate profile, as substantially higher cell death rates were observed (Fig. 1D). In summary, metabolic pathways including glycolysis, TCA cycle, ATP biosynthesis, nitrosylation, and response to oxidative stress were most affected by acute trauma-inflicted protein release. This new data may contribute to a reported energetic and metabolic depression in mechanically traumatized astrocytes in the early hours after TBI (Bartnik et al. 2007; Scafidi et al. 2009).

Trauma-inflicted protein release and cellular depletion were exacerbated by lack of STAT3

Proteomic changes were validated using Western blotting for 13 proteins, selected based on their enrichment in astrocytes (Cahoy et al. 2008) or due to genotype differences (Fig. 2B). CON cells, not STAT3-CKO cells, rapidly increased cellular levels of GFAP, PEA15 and vinculin (VINC) by 30 min after stretching compared to unstretched cells (Fig. 4B, see also Fig. 7A, B). GFAP increase reflects fast post-translational modification rather than *de novo* synthesis (see Discussion). PEA15 and VINC increases are new findings. Trauma-release ("fluid") and cellular reduction ("cells") were determined at 30 min and 5 h post-stretching for both genotypes (Fig. 4B). Repeated immuno-blots confirmed robust fluid elevation for all 13 proteins at both time points post-injury, except SODC in CON fluid, which was elevated only 5 h after stretching (Fig. 4B, Fig. $2D_2$). Representative immunoblots for 9 proteins are shown, either at 30 min (Figs. 4A, 7A, B), with similar release by 5 h after stretching (not shown), or, at 5 h (Figs. 2D, 6A), with similar release already at 30 min post-injury (not shown).

Cellular protein levels did not decrease markedly at 30 min after stretching in CON cell lysates collectively (Fig. 4B); while protein changes in individual cells are addressed below. By 5 h post-injury, CON astrocytes had reduced cellular levels for transgelin (TAGL), CRYAB and 1433E (Fig. 4B, blots not shown). In contrast, stretched STAT3-CKO cells had already by 30 min reduced cellular levels of SODC, VINC, 1433E and GAPDH and additional proteins were reduced by 5 h post-injury including PEA15 (Figs. 4A, B, 7A). Most proteins were reduced in STAT3-CKO astrocytes compared to unstretched levels, except GFAP and ACTB (Fig. 4B, blots shown in Figs. $6A_1$, 7B). Thus, our approach documents for the first time a substantial protein flux from cells to fluids acutely after traumatic astrocyte injury, which was greater in STAT3-CKO versus CON cultures.

Immunoblots show that STAT3-CKO cultures released larger amounts of GAPDH than CON cultures and had greater depletion of cellular GAPDH levels post-injury (Figs. $4A_1$, 4B). ACTN4 release was also larger in stretched STAT3-CKO versus CON cultures, with cellular post-injury levels unchanged at first in both genotypes, but reduced by 5 h in STAT3-CKO stretched cells (Fig. $4A_2$, B). LDHB had lower signal in STAT3-CKO versus CON cells by 5 h post-injury, yet fluid signals were similar in both genotypes but unstretched LDH base expression was reduced in STAT3-CKO versus CON astrocytes (Fig.

4A$_3$, 5B). This prompted us to compare base protein expression in the two genotypes (Fig. 5). Proteins with consistently lower expression in STAT3-CKO compared to CON astrocytes included GFAP, ALDOC, LDHB and PEA15 (Figs. 4A$_3$, 5A$_1$, B and 7A, B). GFAP expression is reported to be regulated by STAT3 activation (Sriram et al. 2004; Herrmann et al., 2008), whereas ALDOC, PEA15 and LDHB are novel STAT3-dependent astrocytic proteins. Expression of GAPDH, TPM4 and ACTN4 was higher in STAT3-CKO versus CON astrocytes, suggesting that these targets were suppressed by STAT3 (Figs. 5A$_2$, B, 4A$_{1–2}$). Alternatively, they could have been increased to compensate for downregulated proteins in STAT3-CKO cells (Di Domenico et al. 2010; Herrmann et al. 2008, Fig. 5B). The covariation factor plot segregated CON and STAT3-CKO by two underlying factors. PEA15, LDHB and ALDOC made Factor 1, while TPM4, GAPDH, ACTN4 and GFAP made a second factor. Together these two factors segregated astrocytes by their genotype with CON astrocytes showing higher values for factor 1 and STAT3-CKO showing higher values for Factor 2, supporting a role for STAT3 in regulating these proteins.

To correlate genotype and trauma induced protein release amounts, we chose 5 proteins with similar base expression in the two genotypes (Fig. 5B). SODC, ACTB, VINC, CRYAB and TAGL release was larger in stretched STAT3-CKO versus CON cultures at either or both post-injury times (Figs. 2C$_2$, D$_2$, 6A, B). Cellular levels for SODC, CRYAB, TAGL and VINC decreased further after injury in STAT3-CKO than in CON cells, except those of ACTB that were saturated (Figs. 4B, 6A, B). Factor analysis grouped VINC, SODC and CRYAB into Factor 1, yielding higher values for STAT3-CKO than CON cells, thereby segregating the genotypes in the factor plot. This demonstrates trauma-inflicted protein covariance based on genotype. We next correlated acute post-injury release of SODC with delayed cell death rates in CON and STAT3-CKO astrocytes (Fig. 6D). Less SODC release acutely post-injury associates with lower cell death rates in CON cells, whereas larger acute SODC release associates with higher delayed cell death rates in STAT3-CKO astrocytes. Together, these data support the idea that acute fluid levels of these markers can signify the magnitude of astrocyte loss, an outcome measure of this injury model.

PEA15 and GFAP loss and breakdown in membrane-injured astrocytes are exacerbated by STAT3 deletion

CON cells increased PEA15 and GFAP signals 30 min after stretching but not STAT3-CKO cells (Figs. 4B, 7A, B). PEA15 fluid levels were similar in both genotypes, whereas those of GFAP were lower in STAT3-CKO versus CON stretched cultures (Fig. 7A, B). In addition to the 50 kDa full size GFAP, stretched CON cells showed a 47 kD GFAP and fluids showed a 37 kD sized GFAP specific signal (Fig. 7B). These proteolytically cleaved GFAP fragments are reported after calcium dependent GFAP proteolysis of *in situ* degraded spinal cord tissue and cultured cortical astrocytes (Ciesielski-Treska et al. 1984; DeArmond et al. 1983).

To better understand these patterns, we analyzed membrane leakage using PI-uptake and monitored it with PEA15 and GFAP staining in individual cells. Uniform PEA15 expression in all unstretched astrocytes changed into a patchwork of PEA15-positive and -negative cells acutely after stretching, documenting striking diversity of PEA15 absence and presence

among injured astrocytes (Fig. 7D). For GFAP, we found 84% of CON unstretched astrocytes expressed GFAP as reported (Fig. 9A, Chiu et al. 1981). Stretching caused GFAP loss and staining changes that were consistent with filament disassembly (see Methods) and associated with permeable cells (Table 5), suggesting post-translational modifications in response to cell wounding (Fig. $7C_2$, $E_{3,4}$). Bright GFAP signals after stretching resemble those seen rapidly after elevating intracellular calcium levels (Lee et al. 2000). Stretched astrocytes with intact membranes retained PEA15 and GFAP was filamentous. Some permeable cells lacking PEA15 still showed GFAP, but with disassembled filaments (Fig. $7D_{3,4}$, $E_{3,4}$). By 48 h post-injury, CON cultures displayed reactive astrocytes with elongated thick processes and elevated PEA15 and GFAP expression compared to signals in unstretched astrocytes and PI-stained nuclei indicated dead astrocytes (see Methods, Fig. $7D_{5,6}$, $E_{5,6}$).

Quantifying cell integrity, fates, and marker pattern showed that stretching caused PEA15 loss in 20% of CON and 40% of STAT3-CKO astrocytes (Figs. 1, 8A, Table 4). Most stretched astrocytes retaining PEA15 had intact membranes while the majority of PEA15 depleted astrocytes were permeable in both genotypes except 22% of CON astrocytes that displayed intact membranes (Fig. $8B_{1,2}$, Table 4). These cells might have been leaky during stretch, released PEA15, and resealed prior to the permeability assay. Time-lapse imaging showed fast resealing after stretching in a similar fraction of injured astrocytes that endure after rhodamine-dextran uptake as “resealed injured” cells (Fig. 1). Together, immunoblot and cell population analyses conclude that PEA15 was released from twice as many STAT3-CKO than CON astrocytes, resulting in similar PEA15 fluid signals in STAT3-CKO and CON stretched cultures despite lower PEA15 ‘base’ expression in STAT3-CKO astrocytes (Fig. 7A).

There were significantly fewer GFAP-positive cells in STAT3-CKO versus CON cultures (Table 5, Fig. 9A). A notable group of STAT3-CKO astrocytes displayed mislocalized GFAP that did not form filaments, but appeared as granular aggregates similar to those found in inclusion bodies (Franke et al. 1982). Resulting Filamentous GFAP-positive population of CON astrocytes was 83% and 48% of STAT3-CKO unstretched astrocytes, excluding cells with granular GFAP distribution (Figs. $7C_1$, 9 A, Table 5). Stretching reduced the GFAP-positive CON population to nearly half and lowered it by one-third in STAT3-CKO cultures (Fig. 9A, Table 5). Thus, lower GFAP fluid levels in STAT3-CKO versus CON cultures were due to release from fewer cells of a smaller GFAP-positive population with lower GFAP expression (Figs. 7B, 9A). Surprisingly, stretch-induced GFAP depletion occurred in twice as many cells as PEA15 depletion (Tables 4, 5, Figs. 8A, 9A, $P<0.01$, Tukey). Permeabilizing astrocytes is reported to result in varying depletion ratios of different astrocytic proteins, the cause of which is unknown (Karl et al. 2000, see Discussion).

GFAP loss and filament disassembly resulted in a residual 25% of cells with regular, filament assembled GFAP in CON and only 8% in STAT3-CKO cultures acutely after stretching (Table 5, Fig. 9A). In STAT3-CKO cultures, cell with disassembled GFAP were present in similar fractions acute and two days post-injury, while their fraction decreased in CON cultures by 2 days after stretching ($P<0.05$, Tukey, Table 5). Over the same time

period CON cultures showed a 27% increase in cells with assembled GFAP filaments ($P<0.05$, Tukey, Table 5). To what extent new GFAP expression in reactive astrocytes and filament reconstruction in injured cells contribute to this 'recovery' remains to be determined.

We next correlated membrane integrity with GFAP filament assembly after injury. Almost a quarter of CON and nearly half of STAT3-CKO GFAP expressing cells were permeable acutely after injury (Fig. 9B, Table 5). Most cells with intact membranes had filamentous GFAP whereas the largest fraction of permeable cells was among astrocytes bearing disassembled GFAP in both genotypes acutely after stretching (Fig. 9B). A small cell fraction with bright GFAP signals had highest permeability rates (Table 5, $P< 0.05$, Tukey). Thus, astrocytes with disassembled GFAP filaments and altered GFAP antigenicity associated with membrane wounding acutely post-injury. GFAP was more frequently retained in permeable cells than PEA15, but cellular GFAP underwent these structural changes after injury (Tables 4, 5, Figs. 8B, 9B, $P<0.01$, Tukey). In sum, mechanical trauma inflicted membrane wounding in a subpopulation of homogeneous astrocytes that affected astroglial markers PEA15 and GFAP differently in release, breakdown and cellular organization.

STAT3 impact on histopathology of injured and reactive astrocytes

Studies on acutely injured astrocytes are sparse compared to reports on reactive gliosis. To begin investigating astroglial cell injury and distinguish injured from reactive astrocytes, we chose a well-characterized moderate crush spinal cord injury (SCI) model (Faulkner et al. 2004; Herrmann et al. 2008; Wanner et al. 2013). This model has the advantage that reactive gliosis and scar formation are structurally, temporally and spatially well-defined (Wanner et al., 2013). To this end, we first identified structural features that distinguished acutely injured from reactive astrocytes; we then analyzed selected trauma release markers in pathologically defined astrocytes after crush SCI (see below).

Damaged tissue with injured and dead astrocyte profiles was identified 3 days after SCI when it was easily distinguished from the surrounding penumbra populated by reactive astrocytes (Fig. 10A). Reactive astrocytes typically had hypertrophied cell bodies and thickened processes (Fig. 10D), whereas damaged gray matter tissue near the lesion had astroglial debris and astrocytes with truncated processes (Fig. 10C). Injured white matter tissue contained more astrocytes with tortuous, beaded or disintegrated processes (Fig. 10C), reminiscent of diffuse axonal injury after mechanical shear forces that have been rarely described in traumatically injured astrocytes (Colombo et al. 1997; Farkas et al. 2006).

Both genotypes had pathologically swollen astrocytes with disproportionally enlarged cell bodies and thin or shortened processes in damaged gray matter tissues 6 h after SCI, but they were larger in STAT3-CKO than in CON damaged gray matter (Fig. 11A). By 1 day post-injury most STAT3-CKO astrocytes were absent in injured gray matter and few remaining astrocytes were degenerating while CON astrocytes endured (Fig. 11A). Injured white matter contained reactive and damaged astrocytes with tortuous and beaded processes in CON cords, while reactive astrocytes were missing in STAT3-CKO cords (Fig. 11B). STAT3-CKO white matter damage zones extended 1.7 fold further from the lesion center

into adjacent neural tissues than CON damage zones (Fig. 11C). Poor recovery of STAT3-CKO mice after crush SCI is reported (Herrmann et al. 2008; Wanner et al. 2013). We now document larger damage zones and more prominent *acute* astroglial pathology and demise in STAT3-CKO versus CON injured cords, providing evidence for a role of STAT3 in astrocyte survival.

Trauma-release markers distinguish STAT3 mediated reactivity and injury

After quantifying injured cell populations and their marker release into fluids in vitro, we next addressed whether the identified release markers are present in the crushed spinal cord, providing polarity of a defined injury site. Presence of four astrocyte enriched trauma-release markers was determined in uninjured, injured and reactive astrocytes at the cellular level, rather than by immunoblotting of tissue homogenates to avoid inconsistent tissue compositions after SCI between the two genotypes (Wanner et al. 2013) and to investigate different cell fates and markers coexisting in neighboring areas. Acutely after SCI, injured astrocytes were located near the lesion, while reactive astrocytes in CON cords were more distally around the lesion (see Fig. 10). In uninjured spinal cords ALDOC was robustly expressed in CON astrocytes, but signals were weak in STAT3-CKO astrocytes, supporting the relevance of in vitro quantified STAT3-dependent ALDOC expression (Figs. 12A, 5). Cytosolic ALDOC colocalized with GFAP, but ALDOC was also present in cell bodies and fine process endings, making it a useful astrocyte-specific marker. PEA15 showed expression in some uninjured CON astrocytes, but signals were weak in STAT3-CKO astrocytes (Fig. 12B). In uninjured mouse spinal cords CRYAB was not colocalized with GFAP expressing astrocytes of either genotype (Fig. 12C). CRYAB was chosen based on its role after SCI and its interaction with GFAP (see below, Klopstein et al. 2012; Koyama and Goldman 1999).

After SCI, ALDOC signal was depleted in injured astrocytes near the lesion at 6 hr post-SCI, but was present in enlarged cell bodies of injured astrocytes one day later (Fig. 13A and insert). Reactive astrocytes in the penumbra had strong ALDOC and GFAP expression (Fig. 13A). Injured STAT3-CKO astrocytes extended farther in lesioned cords and had only marginal ALDOC signals (Figs. 11C, 13A). PEA15 was depleted 6 h after injury (Fig. 13B, insert). By one day post-SCI, few injured CON astrocytes displayed marginal PEA15 signal, while it was expressed in reactive astrocytes distal from the lesion (Fig. 13B). STAT3-CKO, injured astrocytes had marginal PEA15 signals (Fig. 13B). Thus, ALDOC and PEA15 are newly in vivo confirmed STAT3 regulated astrocyte markers in addition to GFAP (Herrmann et al. 2008; Wanner et al. 2013). They are acutely lost from injured astrocytes, but robustly expressed in territorial, reactive astrocytes after SCI, serving as new markers for reactive gliosis.

At 6 h after SCI near the lesion, injured astrocytes clearly expressed CRYAB in both genotypes (Fig. 13C). In contrast, no reactive astrocytes expressed detectable CRYAB (Fig. 13C). CRYAB was colocalized with GFAP in pathologically swollen astrocytes with pruned processes (Fig. 13B and insert). In these astrocytes reduced GFAP signals appeared faint and fragmented resembling stains in injured astrocytes after stretching (Figs. 13C, 7C, E). CRYAB associates with GFAP in pathological aggregates called Rosenthal fibers and it has

a function in regulating GFAP assembly (Hagemann et al. 2009; 2006). CRYAB expression remained in injured astrocytes one day post-SCI whereas adjacent reactive astrocytes were CRYAB-negative (Fig. 13C). CRYAB colocalized with decreased GFAP signals in wounded astrocytes supports its acute function as a heat shock protein and cytoskeletal organizer after mechanical trauma. Decreased, filament disrupted GFAP appears as a feature of swollen astrocytes near SCI lesions and mechanoporated astrocytes after stretching (Figs. 7C, E, 9). These mouse SCI data document astroglial marker differences that demonstrate a new biochemical diversity that is related to specific astrocyte states of cell injury and reactivity, which were both affected by the deletion of cell survival-supporting transcription factor STAT3.

DISCUSSION

We used a simple mechanical astrocyte trauma model with and without STAT3 deletion, measured proteome profiles, and identified proteins released after pressure-pulse stretching. Cell fate after trauma was related to release profiles that reflect cell injury, mechanoporation, and cellular outcomes of survival, reactivity and cell death. Our studies are the first to reveal subpopulations of traumatized astrocytes based on proteome profiles and specific astrocytic marker elevation, depletion and post-injury modification that were validated *in vivo*. This work will help elucidate a signature of astrocyte injury and demise in biofluids after CNS trauma. Our results showed that astrocytes responded with mixed vulnerability to mechanical trauma, which we have begun to investigate *in vivo*.

Trauma causes membrane poration to various extents, leaving a fluid trace and mixed fate

Mechanical trauma causes temporary and different degrees of plasma membrane wounding (Barbee 2005) that can explain the large variability observed in culture trauma models (Cullen et al. 2011; Geddes et al. 2003;). Various injury responses and cell fates are systematically documented as a homogeneous astrocyte population that turns into a mosaic of intact, permeable, resealed and dead cells after a simple mechanical trauma pulse, a finding relevant to acute in vivo traumatic brain and spinal cord injuries. Dye-uptake reveals perforated membranes of rat cortical neurons after a traumatic impact with some regaining integrity while others endured plasmalemma wounding or underwent delayed integrity compromise (Farkas et al. 2006). After central cortical fluid percussion populations of rat neurons are acutely porated, reseal, endure or re-open associating with different ultrastructural morphologies including mitochondrial irregularity, vacuolization and neurofilament disassembly (Lafrenaye et al. 2012; Tang-Schomer et al. 2010). Diffuse axonal injury causes axolemmal permeability with swelling and bead formation (Buki and Povlishock 2006; Kilinc et al. 2009). Mechanoporated cells accumulate around the lesion acutely after mouse SCI (Choo et al. 2007). When following porated cells using dye pulse-labeling over time after controlled cortical impact, Whalen and colleagues found dye overlap with pyknotic cells and label disappearance, suggesting wounded mouse cortical cells undergo protracted cell death (Whalen et al. 2008). Thus, acute plasma membrane permeability is a fundamental feature of traumatic CNS injury of unknown mechanism. Acutely after SCI, we show structural astroglial pathology including swelling and process fragmentation and astrocyte membrane wounding after in vitro trauma that associated with

significant protein release into fluids, leaving an injury “trace”. Importantly, this release process reflects the population of injured and dying cells as shown in the proteomic profiles and individual marker levels. Thus, acute biofluid marker elevation captures ensuing astroglial demise with the possibility for future clinical diagnostic use.

STAT3 is a key player in energy metabolism that determines the fate of traumatized astrocytes

Our data suggests an acute role of STAT3 in astroglial resilience to mechanical trauma because its deletion increased necrosis. Failure to undergo apoptosis, an ATP dependent process, is consistent with exacerbated energy deficiency in STAT3 CKO cells compared to non-transgenic astrocytes after trauma. Energy control is critical for cell survival after traumatic injury. Stretched rat cortical astrocytes had vacuolated mitochondria, decreased mitochondrial potential and reduced ATP levels that recovered by 24 h (Ahmed et al. 2000; Ellis et al. 1995). A transient ATP deficit occurs after mechanical injury in rat neurons (Geddes et al. 2003). Mouse cortical neurons show decreased mitochondrial potential after moderate stretching and a failure to recover after a secondary insult (Arundine et al. 2004).

STAT3 has a key function in oxidative metabolism regulating a switch between mitochondrial respiration and cytosolic glycolysis (Reich 2009). Phosphorylated STAT3 is present in mitochondria of cancer and astrocytes (Sarafian et al. 2010; Wegrzyn et al. 2009). STAT3-deficient astrocytes have reduced ATP production, lower mitochondrial membrane potential and glutathione levels, and are vulnerable to glucose restriction and free oxygen radicals (Sarafian et al., 2010). These findings document an essential role of STAT3 for cell survival and metabolic capacity, not addressing the molecular players. Our work extends previous proteomic data on STAT3-deficient mouse neurons reporting changes in metabolic proteins after ischemic injury and oxidative modification of mitochondrial proteins after rat controlled cortical impact (Di Domenico et al. 2012; Opii et al. 2007). Our new data shows lower expression of glucose controlling and metabolizing enzymes, including LDHB, ALDOC and PEA15 in STAT3-deficient astrocytes. In addition, stretching caused greater trauma-release of metabolic enzymes including alpha enolase, transitional ER ATPase and ESTD among others, amounting to an unfavorable energy status and cell death of traumatized STAT3-CKO astrocytes. Thus, the STAT3-goverend metabolic capacity is important for cellular recovery from trauma. Hence, mechanoporation inflicted metabolic enzyme decrease adds to changes in their substrates making traumatized astrocytes vulnerable. A transient ATP deficit and elevated free oxygen radicals further exacerbate a post-traumatic energy deficit (Arundine et al. 2004;). Impaired glucose utilization via oxidative metabolism and a shift to glycolysis occur acutely after trauma and during post-traumatic metabolic depression in rat cortical models of controlled contusion and moderate lateral fluid percussion (Bartnik et al. 2007; Hovda et al. 1991; Scafidi et al. 2009). Thus, understanding acute injury mechanisms and survival strategies of transiently compromised astrocytes in metabolic distress is essential for overcoming a state of metabolic crisis that is found even after mild TBI (Giza and Hovda 2014).

Astrocyte structures and new markers capture injury and reactivity after neurotrauma

Heterogeneous responses to trauma and astrocyte demise after neurotrauma are understudied. Post-injury induction of GFAP expression occurs between 12–24 h after mild cortical contusion in the mouse (Hinkle et al. 1997). Astrocyte injury and death are acute and are followed by reactive gliosis, producing prominent, enlarged and numerous astrocytes around the lesion, masking their preceding astrocyte demise. Significant rat hippocampal astrocyte loss is reported acutely after fluid percussion injury (Zhao et al. 2003). Mouse fibrous astrocyte populations are nearly halved in white matter after contusion SCI (Lytle and Wrathall 2007), while new astrocytes are added by proliferation, a capacity also shared by cortical and hippocampal astrocytes after traumatic injuries (Lytle and Wrathall 2007; Wanner et al. 2013; Topp et al. 1989). Diffuse astrocyte loss is quantitated 6 h onwards after human TBI in postmortem cortical and hippocampal white matter biopsies (Li et al. 2012). Ultrastructure of brain biopsies show extensive astroglial swelling 3 hours to 3 days after cerebral contusion reflecting cytotoxic edema followed by cell death (Bullock et al. 1991). Thus, histopathology documents astroglial demise after neurotrauma, yet without molecular markers. Our work adds molecular properties of traumatized astrocytes including ALDOC and PEA15 depletion as well as CRYAB induction and association with filament-degraded GFAP.

Astrocyte injury and STAT3-regulated proteins

SCI inflicted astrocyte swelling and process beading are pathological features of trauma and of ischemia that has been more extensively studied (Fern et al. 2014; Salter and Fern 2008). The structural and proteomic changes likely reflect a combination of mechanical trauma and a subsequent ischemic episode, both share similar pathology including metabolic depression. Astrocytes are particularly vulnerable to ischemia resulting in cytotoxic edema and energy demise (Cao et al. 2010; Hertz 2008). Degenerating astrocytic processes with swollen endfeet, abnormal mitochondria and GFAP reduction are part of astroglial necrosis after stroke (Ito et al. 2009; Lukaszevicz et al. 2002). Ischemia after middle cerebral artery occlusion induces STAT3 mainly in astrocytes with acute activation in ischemic areas followed by maintained activity over days in reactive astrocytes of neighboring cortical and hippocampal regions (Choi et al. 2003; Justicia et al. 2000). SCI, STAT3-CKO cords had exacerbated astrocytes swelling and necrosis and broader tissue damage and neuronal death than CON cords, thus, STAT3-mediated astrocyte survival is neuroprotective (Wanner et al. 2013). This adds to the previously described neuroprotection of STAT3 activation in rat neurons acutely following focal cerebral ischemia (Dziennis et al. 2007).

In addition to increased protein depletion and metabolic deficit, changes in structural proteins could contribute to the vulnerability of STAT3-deficient, traumatized astrocytes, as they expressed less GFAP (Herrmann et al. 2008; Sarafian et al. 2010). TPM4 and ACTN4 are two actin-regulating proteins that are elevated in STAT3-CKO compared to CON astrocytes and could increase cell rigidity, making the cells more vulnerable. A function of tropomyosin in cell stiffness is consistent with its reduction during shape changes of astrocytes becoming reactive (Canonne-Hergaux et al. 1994; Ferrier et al. 1994). Further studies on cytoskeletal proteins and their regulators are needed to address astrocyte structural resilience to trauma.

Protein-protein interactions determine marker specific release pools

What influences the extent of individual proteins released after trauma? Contributing to a protein's unique "release pool" are its connection to the cytoskeleton, protein complex assembly, cell compartmental residence, molecular weight and varying base expression levels. Differences between PEA15 and GFAP release could be caused by PEA15 association with astrocyte microtubules, thereby diminishing its releasable pool (Estelles et al. 1996). GFAP filaments were disassembled and degraded after stretching; part was released while part remained cellular. Possible causes include elevated intracellular calcium after trauma (Mills et al. 2004; Rzigalinski et al. 1998; Floyd et al. 2001), which is known to mediate GFAP filament degradation (Ciesielski-Treska et al. 1984; DeArmond et al. 1983). GFAP filament assembly is supported by S100β, 14-3-3E and CRYAB (Bianchi et al. 1994; Li et al. 2006; Nicholl and Quinlan 1994; Ellis et al. 2007). Their trauma-release and cellular loss may attenuate GFAP filament assembly. GFAP proteolytic cleavage in human white matter lesions and in degenerated frontal lobes supports its clinical relevance, yet associated pathophysiology needs to be further investigated (Martinez et al. 2008; Newcombe et al. 1986).

Astrocyte marker release profiles present a fluid signature of traumatic injury with potential clinical relevance

Astrocytes are known for shedding vesicles enriched in intracellular proteins, including carbohydrate metabolic enzymes like ALDOC (Sandoval et al. 2013), here identified as an astrocyte trauma-release protein. Proteins released after trauma and via exosomes bypass classical secretory pathways. Exosomes carry trauma-released proteins, and carry altered proteomic profiles in brains of patients with neurodegenerative disease than those of healthy brains (Harrington et al. 2009). Leak of protein-sized dyes occurs also from membrane-wounded Chinese hamster ovary cells (Mellgren et al. 2007). Vesicle-associated protein release occurs during repair of wounded membranes or, as our time-lapse findings indicate, can precede terminal cell lysis (Godell et al. 1997; Lusardi et al. 2003). Thus, fluid-derived astrocytic proteins are released from transiently plasmalemmal-compromised cells via membrane poration, exosome shedding or during necrotic cell lysis. Clinical relevance of astroglial protein release into biofluids is provided by reporting GFAP elevation in CSF and blood of TBI patients (Mondello et al. 2011; Okonkwo et al. 2013; Pelinka et al. 2004). A biofluid signature of astrocyte injury and death is supported by proteomic analyses of individual TBI patient's CSF showing metabolic and astrocytic proteins present in our trauma-release proteome (Hanrieder et al. 2009; Sjodin et al. 2010). We began to explore astrocyte-specific proteins in biofluids of TBI patients revealing a substantial overlap with our mouse astrocyte trauma-release proteome (manuscript in preparation). This work provides a proteomic reference list that captures astroglial injury and cell death after acute trauma and offers new neurotrauma biomarker candidates with potential diagnostic and predictive value for TBI patients.

Acknowledgments

This work was supported by grants from NIH (1R21NS072606 to IBW; R01NS057624 to MVS; R01GM104610 to JAL), the Neilsen Foundation (82776 to IBW), and the Dr. Miriam and Sheldon Adelson Medical Research Foundation (to MVS).

We acknowledge statistical analysis done by Dr. Jeff Gornbein, Statistical Biomathematical Consulting Clinic, Dept. of Biomathematics, UCLA. Further acknowledgement for assistance goes to Anji Li, Nathalie Focha, Melania Apostolidou, Jumana Aljumainy and Julia Halford from the Wanner lab; Donna Crandall at the Semel Institute, Melissa Sondej and Philip Doran of the UCLA Molecular Instrumentation Center, and Yan Ao and Rose Korsak of the Neurobiology Department, Dr. Sofroniew's lab.

References

Ahmed SM, Rzigalinski BA, Willoughby KA, Sitterding HA, Ellis EF. Stretch-induced injury alters mitochondrial membrane potential and cellular ATP in cultured astrocytes and neurons. J Neurochem. 2000; 74(5):1951–60. [PubMed: 10800938]

Arundine M, Aarts M, Lau A, Tymianski M. Vulnerability of central neurons to secondary insults after in vitro mechanical stretch. J Neurosci. 2004; 24(37):8106–23. [PubMed: 15371512]

Barbee KA. Mechanical cell injury. Ann N Y Acad Sci. 2005; 1066:67–84. [PubMed: 16533919]

Bartnik BL, Lee SM, Hovda DA, Sutton RL. The fate of glucose during the period of decreased metabolism after fluid percussion injury: a 13C NMR study. J Neurotrauma. 2007; 24(7):1079–92. [PubMed: 17610349]

Bianchi R, Verzini M, Garbuglia M, Giambanco I, Donato R. Mechanism of S100 protein-dependent inhibition of glial fibrillary acidic protein (GFAP) polymerization. Biochim Biophys Acta. 1994; 1223(3):354–60. [PubMed: 7918670]

Buki A, Povlishock JT. All roads lead to disconnection?--Traumatic axonal injury revisited. Acta Neurochir (Wien). 2006; 148(2):181–93. discussion 193–4. [PubMed: 16362181]

Bullock R, Maxwell WL, Graham DI, Teasdale GM, Adams JH. Glial swelling following human cerebral contusion: an ultrastructural study. J Neurol Neurosurg Psychiatry. 1991; 54(5):427–34. [PubMed: 1865206]

Burda JE, Sofroniew MV. Reactive gliosis and the multicellular response to CNS damage and disease. Neuron. 2014; 81(2):229–48. [PubMed: 24462092]

Cahoy JD, Emery B, Kaushal A, Foo LC, Zamanian JL, Christopherson KS, Xing Y, Lubischer JL, Krieg PA, Krupenko SA, et al. A transcriptome database for astrocytes, neurons, and oligodendrocytes: a new resource for understanding brain development and function. J Neurosci. 2008; 28(1):264–78. [PubMed: 18171944]

Canonne-Hergaux F, Zwiller J, Aunis D. cAMP and bFGF negatively regulate tropomyosin expression in rat cultured astroblasts. Neurochem Int. 1994; 25(6):545–53. [PubMed: 7894331]

Cao X, Zhang Y, Zou L, Xiao H, Chu Y, Chu X. Persistent oxygen-glucose deprivation induces astrocytic death through two different pathways and calpain-mediated proteolysis of cytoskeletal proteins during astrocytic oncosis. Neurosci Lett. 2010; 479(2):118–22. [PubMed: 20493926]

Chiu FC, Norton WT, Fields KL. The cytoskeleton of primary astrocytes in culture contains actin, glial fibrillary acidic protein, and the fibroblast-type filament protein, vimentin. J Neurochem. 1981; 37(1):147–55. [PubMed: 7019391]

Choo AM, Liu J, Lam CK, Dvorak M, Tetzlaff W, Oxland TR. Contusion, dislocation, and distraction: primary hemorrhage and membrane permeability in distinct mechanisms of spinal cord injury. J Neurosurg Spine. 2007; 6(3):255–66. [PubMed: 17355025]

Choi JS, Kim SY, Cha JH, Choi YS, Sung KW, Oh ST, Kim ON, Chung JW, Chun MH, Lee SB, et al. Upregulation of gp130 and STAT3 activation in the rat hippocampus following transient forebrain ischemia. Glia. 2003; 41(3):237–46. [PubMed: 12528179]

Ciesielski-Treska J, Goetschy JF, Aunis D. Proteolytic degradation of vimentin and glial fibrillary acidic protein in rat astrocytes in primary culture. Eur J Biochem. 1984; 138(3):465–71. [PubMed: 6319134]

Colombo JA, Yanez A, Lipina SJ. Interlaminar astroglial processes in the cerebral cortex of non human primates: response to injury. J Hirnforsch. 1997; 38(4):503–12. [PubMed: 9476215]

de Vellis, J.; Ghiani, C.; Wanner, I.; Cole, R. Preparation of Normal and Reactive Astrocyte Cultures. In: Doering, L., editor. Protocols for Neural Cell Culture. Vol. Chapter 9. Totowa, NJ: Humana Press Inc. Springer; 2009. p. 193-216.

DeArmond SJ, Fajardo M, Naughton SA, Eng LF. Degradation of glial fibrillary acidic protein by a calcium dependent proteinase: an electroblot study. Brain Res. 1983; 262(2):275–82. [PubMed: 6340792]

Di Domenico F, Casalena G, Sultana R, Cai J, Pierce WM, Perluigi M, Cini C, Baracca A, Solaini G, Lenaz G, et al. Involvement of stat3 in mouse brain development and sexual dimorphism: a proteomics approach. Brain Res. 2010; 1362:1–12. [PubMed: 20875800]

Dziennis S, Jia T, Ronnekleiv OK, Hurn PD, Alkayed NJ. Role of signal transducer and activator of transcription-3 in estradiol-mediated neuroprotection. J Neurosci. 2007; 27(27):7268–74. [PubMed: 17611279]

Efron B, Tibshirani R. Statistical data analysis in the computer age. Science. 1991; 253(5018):390–5. [PubMed: 17746394]

Ellis EF, McKinney JS, Willoughby KA, Liang S, Povlishock JT. A new model for rapid stretch-induced injury of cells in culture: characterization of the model using astrocytes. J Neurotrauma. 1995; 12(3):325–39. [PubMed: 7473807]

Ellis EF, Willoughby KA, Sparks SA, Chen T. S100B protein is released from rat neonatal neurons, astrocytes, and microglia by in vitro trauma and anti-S100 increases trauma-induced delayed neuronal injury and negates the protective effect of exogenous S100B on neurons. J Neurochem. 2007; 101(6):1463–70. [PubMed: 17403138]

Estelles A, Yokoyama M, Nothias F, Vincent JD, Glowinski J, Vernier P, Chneiweiss H. The major astrocytic phosphoprotein PEA-15 is encoded by two mRNAs conserved on their full length in mouse and human. J Biol Chem. 1996; 271(25):14800–6. [PubMed: 8662970]

Farkas O, Lifshitz J, Povlishock JT. Mechanoporation induced by diffuse traumatic brain injury: an irreversible or reversible response to injury? J Neurosci. 2006; 26(12):3130–40. [PubMed: 16554464]

Faulkner JR, Herrmann JE, Woo MJ, Tansey KE, Doan NB, Sofroniew MV. Reactive astrocytes protect tissue and preserve function after spinal cord injury. J Neurosci. 2004; 24(9):2143–55. [PubMed: 14999065]

Fern RF, Matute C, Stys PK. White matter injury: Ischemic and nonischemic. Glia. 2014; 62(11): 1780–9. [PubMed: 25043122]

Ferrier R, Had L, Rabie A, Faivre-Sarrailh C. Coordinated expression of five tropomyosin isoforms and beta-actin in astrocytes treated with dibutyryl cAMP and cytochalasin D. Cell Motil Cytoskeleton. 1994; 28(4):303–16. [PubMed: 7954857]

Floyd CL, Rzigalinski BA, Weber JT, Sitterding HA, Willoughby KA, Ellis EF. Traumatic injury of cultured astrocytes alters inositol (1,4,5)-trisphosphate-mediated signaling. Glia. 2001; 33(1):12–23. [PubMed: 11169788]

Franke WW, Schmid E, Grund C, Geiger B. Intermediate filament proteins in nonfilamentous structures: transient disintegration and inclusion of subunit proteins in granular aggregates. Cell. 1982; 30(1):103–13. [PubMed: 6751555]

Geddes DM, LaPlaca MC, Cargill RS 2nd. Susceptibility of hippocampal neurons to mechanically induced injury. Exp Neurol. 2003; 184(1):420–7. [PubMed: 14637111]

Gennarelli, TA.; Thibault, LE. Biological models of head injury. In: Becker, DP.; Povlishock, JT., editors. Central Nervous System Traums Status Report-1985. Bethesda, MD: National Inst. of Health; 1985. p. 391-404.

Giza CC, Hovda DA. The new neurometabolic cascade of concussion. Neurosurgery. 2014; 75(Suppl 4):S24–33. [PubMed: 25232881]

Godell CM, Smyers ME, Eddleman CS, Ballinger ML, Fishman HM, Bittner GD. Calpain activity promotes the sealing of severed giant axons. Proc Natl Acad Sci U S A. 1997; 94(9):4751–6. [PubMed: 9114063]

Greco TM, Seeholzer SH, Mak A, Spruce L, Ischiropoulos H. Quantitative mass spectrometry-based proteomics reveals the dynamic range of primary mouse astrocyte protein secretion. J Proteome Res. 2010; 9(5):2764–74. [PubMed: 20329800]

Hagemann TL, Boelens WC, Wawrousek EF, Messing A. Suppression of GFAP toxicity by alphaB-crystallin in mouse models of Alexander disease. Hum Mol Genet. 2009; 18(7):1190–9. [PubMed: 19129171]

Hagemann TL, Connor JX, Messing A. Alexander disease-associated glial fibrillary acidic protein mutations in mice induce Rosenthal fiber formation and a white matter stress response. J Neurosci. 2006; 26(43):11162–73. [PubMed: 17065456]

Hanrieder J, Wetterhall M, Enblad P, Hillered L, Bergquist J. Temporally resolved differential proteomic analysis of human ventricular CSF for monitoring traumatic brain injury biomarker candidates. J Neurosci Methods. 2009; 177(2):469–78. [PubMed: 19263575]

Harrington MG, Fonteh AN, Oborina E, Liao P, Cowan RP, McComb G, Chavez JN, Rush J, Biringer RG, Huhmer AF. The morphology and biochemistry of nanostructures provide evidence for synthesis and signaling functions in human cerebrospinal fluid. Cerebrospinal Fluid Res. 2009; 6:10. [PubMed: 19735572]

Herrmann JE, Imura T, Song B, Qi J, Ao Y, Nguyen TK, Korsak RA, Takeda K, Akira S, Sofroniew MV. STAT3 is a critical regulator of astrogliosis and scar formation after spinal cord injury. J Neurosci. 2008; 28(28):7231–43. [PubMed: 18614693]

Hertz L. Bioenergetics of cerebral ischemia: a cellular perspective. Neuropharmacology. 2008; 55(3): 289–309. [PubMed: 18639906]

Hinkle DA, Baldwin SA, Scheff SW, Wise PM. GFAP and S100beta expression in the cortex and hippocampus in response to mild cortical contusion. J Neurotrauma. 1997; 14(10):729–38. [PubMed: 9383091]

Hovda DA, Yoshino A, Kawamata T, Katayama Y, Becker DP. Diffuse prolonged depression of cerebral oxidative metabolism following concussive brain injury in the rat: a cytochrome oxidase histochemistry study. Brain Res. 1991; 567(1):1–10. [PubMed: 1667742]

Ito U, Hakamata Y, Kawakami E, Oyanagi K. Degeneration of astrocytic processes and their mitochondria in cerebral cortical regions peripheral to the cortical infarction: heterogeneity of their disintegration is closely associated with disseminated selective neuronal necrosis and maturation of injury. Stroke. 2009; 40(6):2173–81. [PubMed: 19359621]

Justicia C, Gabriel C, Planas AM. Activation of the JAK/STAT pathway following transient focal cerebral ischemia: signaling through Jak1 and Stat3 in astrocytes. Glia. 2000; 30(3):253–70. [PubMed: 10756075]

Karl J, Gottfried C, Tramontina F, Dunkley P, Rodnight R, Goncalves CA. GFAP phosphorylation studied in digitonin-permeabilized astrocytes: standardization of conditions. Brain Res. 2000; 853(1):32–40. [PubMed: 10627305]

Kazanis I. CNS injury research; reviewing the last decade: methodological errors and a proposal for a new strategy. Brain Res Brain Res Rev. 2005; 50(2):377–86. [PubMed: 16274749]

Kilinc D, Gallo G, Barbee KA. Mechanical membrane injury induces axonal beading through localized activation of calpain. Exp Neurol. 2009; 219(2):553–61. [PubMed: 19619536]

Klopstein A, Santos-Nogueira E, Francos-Quijorna I, Redensek A, David S, Navarro X, Lopez-Vales R. Beneficial effects of alphaB-crystallin in spinal cord contusion injury. J Neurosci. 2012; 32(42): 14478–88. [PubMed: 23077034]

Koyama Y, Goldman JE. Formation of GFAP cytoplasmic inclusions in astrocytes and their disaggregation by alphaB-crystallin. Am J Pathol. 1999; 154(5):1563–72. [PubMed: 10329608]

Kwon BK, Casha S, Hurlbert RJ, Yong VW. Inflammatory and structural biomarkers in acute traumatic spinal cord injury. Clin Chem Lab Med. 2011; 49(3):425–33. [PubMed: 21175377]

Lafrenaye AD, McGinn MJ, Povlishock JT. Increased intracranial pressure after diffuse traumatic brain injury exacerbates neuronal somatic membrane poration but not axonal injury: evidence for primary intracranial pressure-induced neuronal perturbation. J Cereb Blood Flow Metab. 2012; 32(10):1919–32. [PubMed: 22781336]

Lee YB, Du S, Rhim H, Lee EB, Markelonis GJ, Oh TH. Rapid increase in immunoreactivity to GFAP in astrocytes in vitro induced by acidic pH is mediated by calcium influx and calpain I. Brain Res. 2000; 864(2):220–9. [PubMed: 10802029]

Li DR, Zhang F, Wang Y, Tan XH, Qiao DF, Wang HJ, Michiue T, Maeda H. Quantitative analysis of GFAP- and S100 protein-immunopositive astrocytes to investigate the severity of traumatic brain injury. Leg Med (Tokyo). 2012; 14(2):84–92. [PubMed: 22301378]

Li H, Guo Y, Teng J, Ding M, Yu AC, Chen J. 14-3-3gamma affects dynamics and integrity of glial filaments by binding to phosphorylated GFAP. J Cell Sci. 2006; 119(Pt 21):4452–61. [PubMed: 17032734]

Lubieniecka JM, Streijger F, Lee JH, Stoynov N, Liu J, Mottus R, Pfeifer T, Kwon BK, Coorssen JR, Foster LJ, et al. Biomarkers for severity of spinal cord injury in the cerebrospinal fluid of rats. PLoS One. 2011; 6(4):e19247. [PubMed: 21559420]

Lukaszevicz AC, Sampaio N, Guegan C, Benchoua A, Couriaud C, Chevalier E, Sola B, Lacombe P, Onteniente B. High sensitivity of protoplasmic cortical astroglia to focal ischemia. J Cereb Blood Flow Metab. 2002; 22(3):289–98. [PubMed: 11891434]

Lusardi TA, Smith DH, Wolf JA, Meaney DF. The separate roles of calcium and mechanical forces in mediating cell death in mechanically injured neurons. Biorheology. 2003; 40(1–3):401–9. [PubMed: 12454433]

Lytle JM, Wrathall JR. Glial cell loss, proliferation and replacement in the contused murine spinal cord. Eur J Neurosci. 2007; 25(6):1711–24. [PubMed: 17432960]

Martinez A, Carmona M, Portero-Otin M, Naudi A, Pamplona R, Ferrer I. Type-dependent oxidative damage in frontotemporal lobar degeneration: cortical astrocytes are targets of oxidative damage. J Neuropathol Exp Neurol. 2008; 67(12):1122–36. [PubMed: 19018247]

Mellgren RL, Zhang W, Miyake K, McNeil PL. Calpain is required for the rapid, calcium-dependent repair of wounded plasma membrane. J Biol Chem. 2007; 282(4):2567–75. [PubMed: 17121849]

Mills LR, Velumian AA, Agrawal SK, Theriault E, Fehlings MG. Confocal imaging of changes in glial calcium dynamics and homeostasis after mechanical injury in rat spinal cord white matter. Neuroimage. 2004; 21(3):1069–82. [PubMed: 15006675]

Mondello S, Papa L, Buki A, Bullock MR, Czeiter E, Tortella FC, Wang KK, Hayes RL. Neuronal and glial markers are differently associated with computed tomography findings and outcome in patients with severe traumatic brain injury: a case control study. Crit Care. 2011; 15(3):R156. [PubMed: 21702960]

Nam S, Buettner R, Turkson J, Kim D, Cheng JQ, Muehlbeyer S, Hippe F, Vatter S, Merz KH, Eisenbrand G, et al. Indirubin derivatives inhibit Stat3 signaling and induce apoptosis in human cancer cells. Proc Natl Acad Sci U S A. 2005; 102(17):5998–6003. [PubMed: 15837920]

Neary JT, Kang Y, Willoughby KA, Ellis EF. Activation of extracellular signal-regulated kinase by stretch-induced injury in astrocytes involves extracellular ATP and P2 purinergic receptors. J Neurosci. 2003; 23(6):2348–56. [PubMed: 12657694]

Newcombe J, Woodroofe MN, Cuzner ML. Distribution of glial fibrillary acidic protein in gliosed human white matter. J Neurochem. 1986; 47(6):1713–9. [PubMed: 3772373]

Nicholl ID, Quinlan RA. Chaperone activity of alpha-crystallins modulates intermediate filament assembly. EMBO J. 1994; 13(4):945–53. [PubMed: 7906647]

Okonkwo DO, Yue JK, Puccio AM, Panczykowski DM, Inoue T, McMahon PJ, Sorani MD, Yuh EL, Lingsma HF, Maas AI, et al. GFAP-BDP as an acute diagnostic marker in traumatic brain injury: results from the prospective transforming research and clinical knowledge in traumatic brain injury study. J Neurotrauma. 2013; 30(17):1490–7. [PubMed: 23489259]

Opii WO, Nukala VN, Sultana R, Pandya JD, Day KM, Merchant ML, Klein JB, Sullivan PG, Butterfield DA. Proteomic identification of oxidized mitochondrial proteins following experimental traumatic brain injury. Journal of Neurotrauma. 2007; 24(5):772–789. [PubMed: 17518533]

Pelinka LE, Kroepfl A, Schmidhammer R, Krenn M, Buchinger W, Redl H, Raabe A. Glial fibrillary acidic protein in serum after traumatic brain injury and multiple trauma. J Trauma. 2004; 57(5): 1006–12. [PubMed: 15580024]

Reich NC. STAT3 revs up the powerhouse. Sci Signal. 2009; 2(90):pe61. [PubMed: 19797267]

Rzigalinski BA, Weber JT, Willoughby KA, Ellis EF. Intracellular free calcium dynamics in stretch-injured astrocytes. J Neurochem. 1998; 70(6):2377–85. [PubMed: 9603202]

Salter MG, Fern R. The mechanisms of acute ischemic injury in the cell processes of developing white matter astrocytes. J Cereb Blood Flow Metab. 2008; 28(3):588–601. [PubMed: 17912272]

Sandoval M, Luarte A, Herrera-Molina R, Varas-Godoy M, Santibanez M, Rubio FJ, Smit AB, Gundelfinger ED, Li KW, Smalla KH, et al. The glycolytic enzyme aldolase C is up-regulated in

rat forebrain microsomes and in the cerebrospinal fluid after repetitive fluoxetine treatment. Brain Res. 2013; 1520:1–14. [PubMed: 23688545]

Sarafian TA, Montes C, Imura T, Qi J, Coppola G, Geschwind DH, Sofroniew MV. Disruption of astrocyte STAT3 signaling decreases mitochondrial function and increases oxidative stress in vitro. PLoS One. 2010; 5(3):e9532. [PubMed: 20224768]

Scafidi S, O'Brien J, Hopkins I, Robertson C, Fiskum G, McKenna M. Delayed cerebral oxidative glucose metabolism after traumatic brain injury in young rats. J Neurochem. 2009; 109(Suppl 1): 189–97. [PubMed: 19393027]

Shen S, Loo RR, Wanner IB, Loo JA. Addressing the needs of traumatic brain injury with clinical proteomics. Clin Proteomics. 2014; 11(1):11. [PubMed: 24678615]

Shevchenko A, Wilm M, Vorm O, Mann M. Mass spectrometric sequencing of proteins silver-stained polyacrylamide gels. Anal Chem. 1996; 68(5):850–8. [PubMed: 8779443]

Shreiber DI, Bain AC, Ross DT, Smith DH, Gennarelli TA, McIntosh TK, Meaney DF. Experimental investigation of cerebral contusion: histopathological and immunohistochemical evaluation of dynamic cortical deformation. J Neuropathol Exp Neurol. 1999; 58(2):153–64. [PubMed: 10029098]

Shu SY, Ju G, Fan LZ. The glucose oxidase-DAB-nickel method in peroxidase histochemistry of the nervous system. Neurosci Lett. 1988; 85(2):169–71. [PubMed: 3374833]

Sjodin MO, Bergquist J, Wetterhall M. Mining ventricular cerebrospinal fluid from patients with traumatic brain injury using hexapeptide ligand libraries to search for trauma biomarkers. J Chromatogr B Analyt Technol Biomed Life Sci. 2010; 878(22):2003–2012.

Sofroniew MV, Vinters HV. Astrocytes: biology and pathology. Acta Neuropathol. 2010; 119(1):7–35. [PubMed: 20012068]

Sondej, M.; Doran, P.; Loo, JA.; Wanner, I. Sample preparation of primary astrocyte cellular and released proteins for 2-D gel electrophoresis and protein identification by mass spectrometry. In: Ivanov, A.; Lazarev, A., editors. Sample preparation in biological mass spectrometry. Dordrecht: Springer; 2011. p. 829-849.

Sriram K, Benkovic SA, Hebert MA, Miller DB, O'Callaghan JP. Induction of gp130-related cytokines and activation of JAK2/STAT3 pathway in astrocytes precedes up-regulation of glial fibrillary acidic protein in the 1-methyl-4-phenyl-1,2,3,6-tetrahydropyridine model of neurodegeneration: key signaling pathway for astrogliosis in vivo? J Biol Chem. 2004; 279(19): 19936–47. [PubMed: 14996842]

Takeda K, Kaisho T, Yoshida N, Takeda J, Kishimoto T, Akira S. Stat3 activation is responsible for IL-6-dependent T cell proliferation through preventing apoptosis: generation and characterization of T cell-specific Stat3-deficient mice. J Immunol. 1998; 161(9):4652–60. [PubMed: 9794394]

Tang-Schomer MD, Patel AR, Baas PW, Smith DH. Mechanical breaking of microtubules in axons during dynamic stretch injury underlies delayed elasticity, microtubule disassembly, and axon degeneration. FASEB J. 2010; 24(5):1401–10. [PubMed: 20019243]

Topp KS, Faddis BT, Vijayan VK. Trauma-induced proliferation of astrocytes in the brains of young and aged rats. Glia. 1989; 2(3):201–11. [PubMed: 2526082]

Wanner IB. An in vitro trauma model to study rodent and human astrocyte reactivity. Methods Mol Biol. 2012; 814:189–219. [PubMed: 22144309]

Wanner IB, Anderson MA, Song B, Levine J, Fernandez A, Gray-Thompson Z, Ao Y, Sofroniew MV. Glial scar borders are formed by newly proliferated, elongated astrocytes that interact to corral inflammatory and fibrotic cells via STAT3-dependent mechanisms after spinal cord injury. J Neurosci. 2013; 33(31):12870–86. [PubMed: 23904622]

Wanner IB, Deik M, Torres M, Rosendahl AR, Neary JT, Lemmon VP, Bixby JL. A new in vitro model of the glial scar inhibits axon growth. Glia. 2008; 56(15):1691–1709. [PubMed: 18618667]

Wegrzyn J, Potla R, Chwae YJ, Sepuri NB, Zhang Q, Koeck T, Derecka M, Szczepanek K, Szelag M, Gornicka A, et al. Function of mitochondrial Stat3 in cellular respiration. Science. 2009; 323(5915):793–7. [PubMed: 19131594]

Whalen MJ, Dalkara T, You Z, Qiu J, Bermpohl D, Mehta N, Suter B, Bhide PG, Lo EH, Ericsson M, et al. Acute plasmalemma permeability and protracted clearance of injured cells after controlled cortical impact in mice. J Cereb Blood Flow Metab. 2008; 28(3):490–505. [PubMed: 17713463]

Zhao X, Ahram A, Berman RF, Muizelaar JP, Lyeth BG. Early loss of astrocytes after experimental traumatic brain injury. Glia. 2003; 44(2):140–52. [PubMed: 14515330]

Main Points

- Mechanically traumatized astrocytes leak proteins into surrounding fluids.
- The fluid derived astroglial trauma-release proteome captures profiles of astrocyte injury and cell death.
- STAT3 regulates cell survival based on the energy capacity of injured astrocytes.

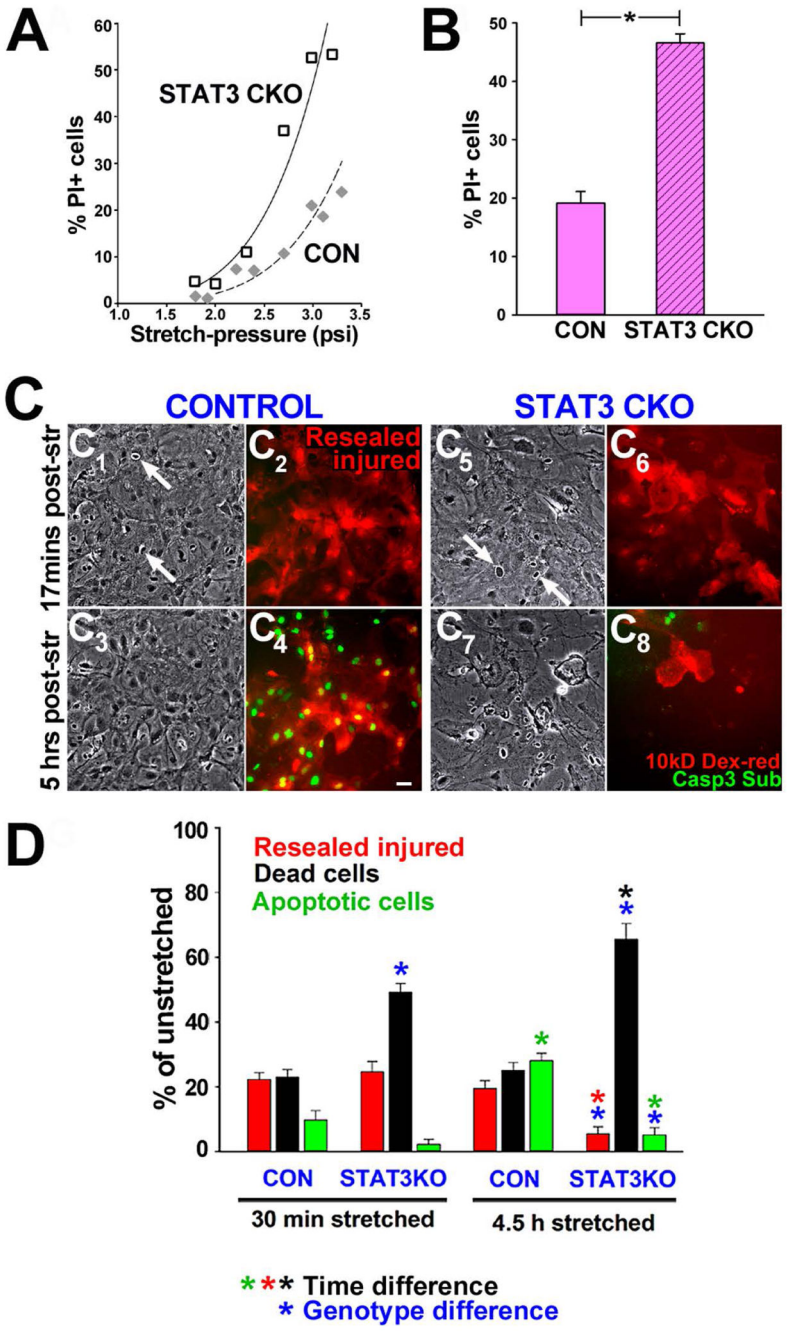

Figure 1. Astrocyte stretch-injury causes acute membrane permeability and cell death that is exacerbated by STAT3 deletion

A, Increasing pressure-stretch intensities (psi) caused proportional elevation in percent unfixed cells taking up propidium iodine (PI) at 48 h post-injury. Severity dependent cell death rates raised higher in conditional STAT3-deleted astrocytes (STAT3-CKO) compared to non-transgenic control (CON) astrocytes. ***B***, Average percent PI-positive cells 48h after stretching at 2.4 ± 0.3 psi was over twofold higher in STAT3-CKO versus CON astrocytes ($P<0.001$, Student's T-test, SEM, cultures of 8 mice each genotype). ***C***, Mechanoporation during stretching, necrosis and apoptosis are monitored using time-lapse video frames of

stretched CON ***(C1–C4)*** and STAT3-CKO ***(C5–C8)*** astrocytes at 17 min ***(C1, 2, 5, 6)*** and at 5 h post-injury ***(C3, 4, 7, 8).*** Phase contrast images show viable cells (gray) and necrotic nuclei of lysed cells (phase-dark with white ring, arrows, ***C1, 3, 5, 7)***. Membrane permeability during stretching led to uptake of 10 kD dextran rhodamine present only during stretching. Retained dye after wash-out indicated membrane resealing (“Resealed injured”, red cells, ***C2, 4, 6, 8)***. Caspase 3 substrate was added prior imaging and was converted into green fluorescence over time in nuclei of apoptotic cells (green, ***C4, 8).*** Bar = 20 μm. ***D,*** Fractions of resealed injured (red), necrotic (black) and apoptotic (green) cells at 30 min and 4.5 h post-injury in CON and STAT3-CKO astrocytes. Necrosis rates (black) were doubled by 30 min and nearly tripled by 4.5 h post-injury in STAT3-CKO compared to CON cultures (blue asterisks, $P < 0.001$, post-hoc multiple comparison ANOVA, Tukey). Resealed injured STAT3-CKO astrocytes underwent significant cell integrity loss between 30 min and 4.5 h post-injury (red asterisk)that was associated with elevated cell death (black asterisk, $P < 0.01$). In contrary, the rate of CON resealed injured astrocytes remained unchanged over this time post-injury (blue asterisk). Delayed apoptosis increased by 4.5 h post-injury in CON, but not in STAT3-CKO cells (blue and green asterisks, $P<0.01$, n=6–7 stretched, n=4 unstretched cultures from mice of each genotype).

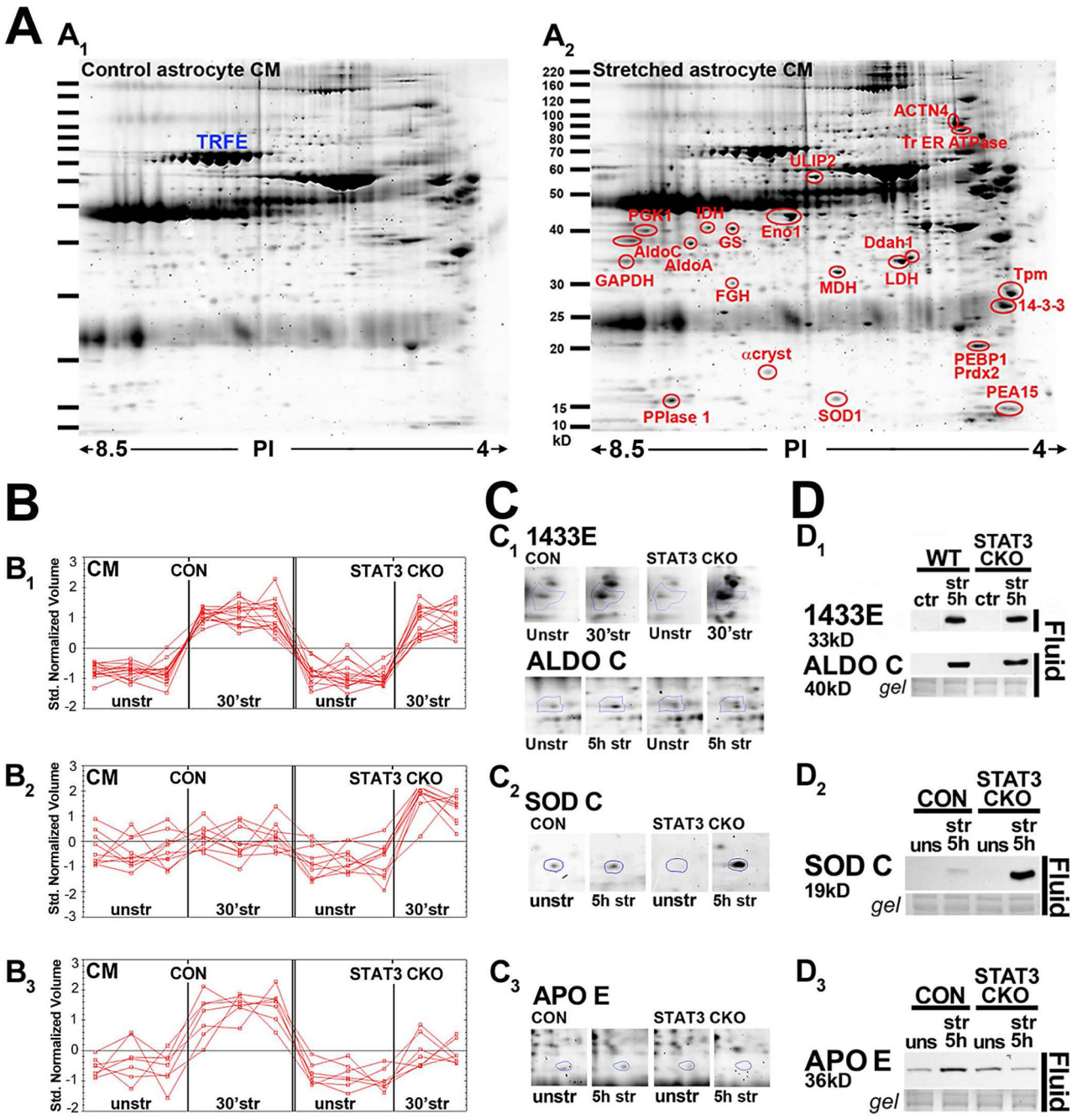

Figure 2. Proteomics of astrocyte trauma-released proteins shows STAT3 dependent profiles

A, Sypro ruby stained 2D gels of conditioned media (CM) from unstretched (***A1***) and stretched (***A2***) astrocytes 5 h post-injury show well separated proteins between 15 and 100 kD. Selected, significantly elevated proteins after stretching are circled (red), while others were unchanged (Transferrin, TRFE ***A1***, blue, ***A2***, red, ≥ 1.8 x; P ≤ 0.05, Table 3). ***B***, Plotted are CM (fluid) protein changes 30 min post-injury grouped into three different release patterns ***(B1–B3)***, each red line showing triplicate spot measures per conditions. ***(B1)*** Similar protein elevation in CM of both genotypes. (***B2***) Post-injury protein CM elevation in

STAT3-CKO, but less or no change in CON cultures; (***B*****3**) Post-injury protein CM elevation in CON but less or no change in STAT3-CKO cultures. ***C***, Examples of Sypro ruby stained CM protein spots that follow the in B plotted release patterns ***(C*****1**–***C*****3)**. (***C*****1)** Levels of Ywhae 14-3-3 ε (1433E at 30 min) and those of Aldolase C (ALDOC, at 5 h) after stretching increased in fluids (CM) of CON and STAT3-CKO cultures. (***C*****2)** [Copper-zinc] superoxide dismutase (SODC) was further elevated in fluids of STAT3-CKO compared to CON cultures at 5 h post-injury. (***C*****3)** CON astrocytes secreted more apolipoprotein E (APO E) into fluids than STAT3-CKO astrocytes by 5 h after stretching. ***D***, Immunoblots of same proteins as in C showing unstretched and 5 h post-stretched fluid signals for both genotypes. ***(D*****1)** 1433E and ALDOC had similar fluid signals in both genotypes. ***(D*****2)** Substantially larger fluid SODC signals are shown in STAT3-CKO versus CON cultures. (***D*****3)** APOE secretion was elevated in CON but reduced in STAT3-CKO stretched cultures.

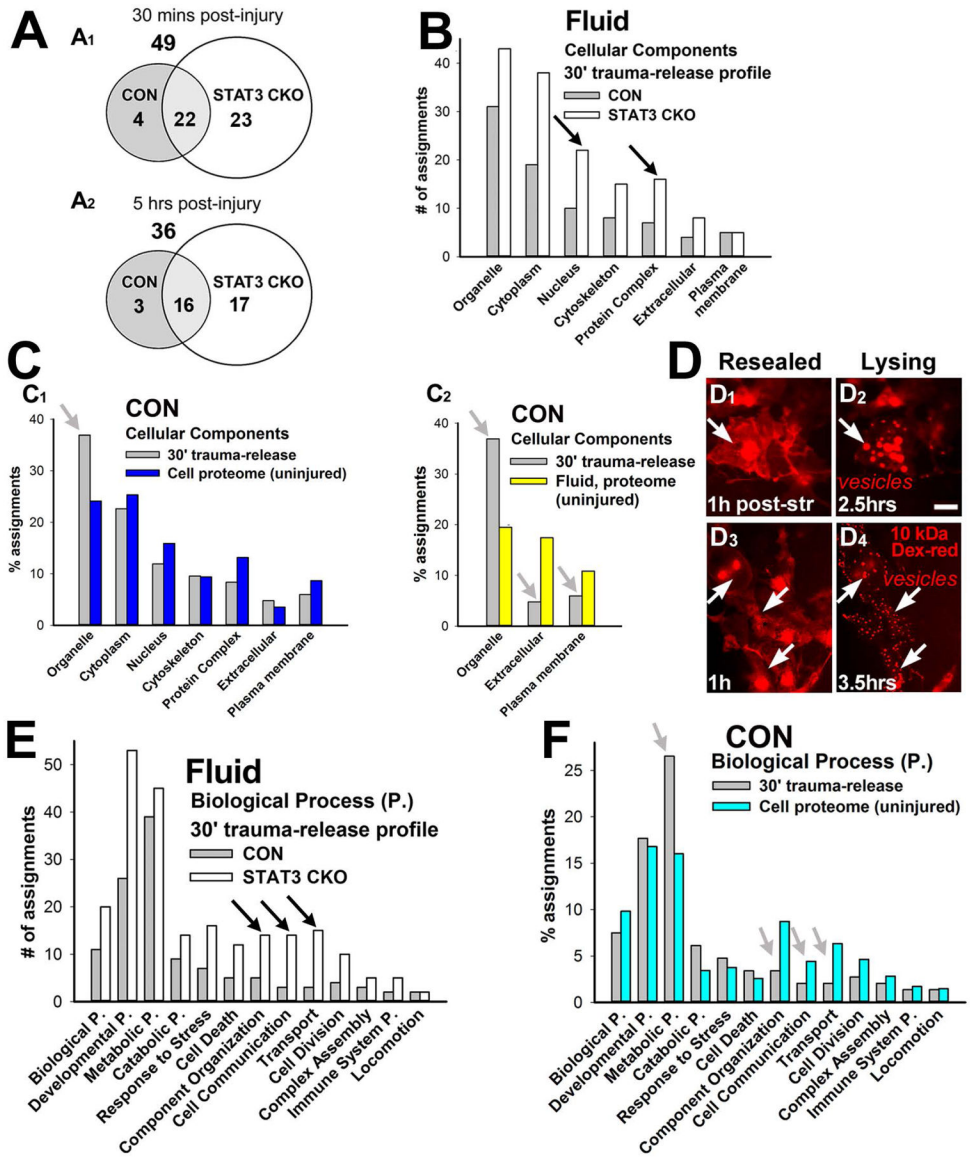

Figure 3. Gene ontology analyses of the astrocyte trauma-release proteome

A, Venn diagrams show numbers of trauma-released proteins by 30 min (***A*** $_{1}$) and by 5 h (***A*** $_{2}$) post-injury from CON and STAT3-CKO cultures. STAT3-CKO astrocytes released 1.6 fold more proteins at 30 min and twice as many at 5 h after injury versus CON stretched astrocytes. ***B***, Number of gene ontology (GO) cellular component assignments of proteins that were released into fluids indicate proportionally more nuclear proteins and protein complexes were released from STAT3-CKO (white) versus CON (gray) cultures 30 min post-injury (black arrows). Protein complex is a stable set of two or more polypeptide subunits. ***C,*** Percent GO assignments of CON trauma-release proteome 30 min post-injury (gray) compared to cellular (***C*** $_{1}$, blue) and fluid proteomes (***C*** $_{2}$, yellow) from unstretched non-transgenic cultures. Organelle-residing proteins were overrepresented whereas extracellular and plasma membrane proteins were underrepresented in the trauma-release proteome (gray arrows). ***D***, Time-lapse images show two post-injury stages: membrane

compromised CON cells that regained integrity shown at one h post-injury (“resealed”, arrows: cytosolic dextran-rhodamine, ***D*$_{1+3}$)**; and same cells undergoing secondary cell integrity loss (“lysing”), associated with vesicle formation at 2.5 h ***(D*$_{2}$)** and 3.5 h ***(D*$_{4}$)** post-stretching (arrows: vesicular dextran-rhodamine) that was followed by dye disappearance (not shown). Bar = 20 μm. ***E,*** CON (gray) and STAT3-CKO (white) trauma-released protein numbers assigned to biological processes. Compared to stretched CON cultures, STAT3-CKO cultures released overall more proteins to significant levels and proportionally more proteins from categories of component organization, cell communication and transport (black arrows). Component Organization describes the process involved in the assembly or disassembly of cellular constituents. ***F,*** Percent protein assignments to biological processes are compared between trauma-released proteins (gray) and the cellular proteome of unstretched non-transgenic astrocyte cell lysates (turquoise). Proteins associated with metabolic and catabolic processes are overrepresented, while proteins of component organization, cell communication and transport are underrepresented in the CON acute trauma-release proteome compared to the cellular proteome.

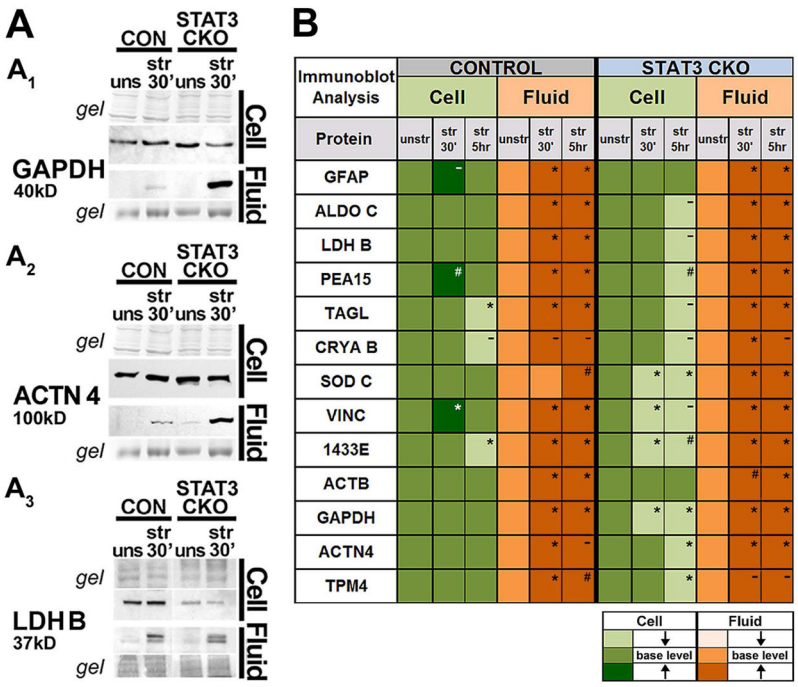

Figure 4. Validation of trauma-induced protein release and STAT3 dependent cellular depletion

A, Gel and immunoblot images show whole cell lysate (cell) and CM (fluid) samples of unstretched and stretched CON and STAT3-CKO astrocytes probed for GAPDH (***A1***), α actinin 4, ACTN4 (***A2***) and lactate dehydrogenase B chain, LDHB (***A3***). ***B,*** Average signal intensity changes of stretched (30 min and 5 h post-injury) versus unstretched signals (≥0.5, see Methods) for 13 proteins (n = 3–6 mice of each genotype per protein). Injury caused fluid protein increases (darker orange) and cellular protein decreases (lighter green) from unstretched signals (base level). Averages of repeatedly observed protein amount differences (≥0.5) in stretched versus unstretched were significant (* with P values <0.001 to <0.05), likely (# with P values <0.08) or not significant (−) determined using repeated measurement ANOVA.

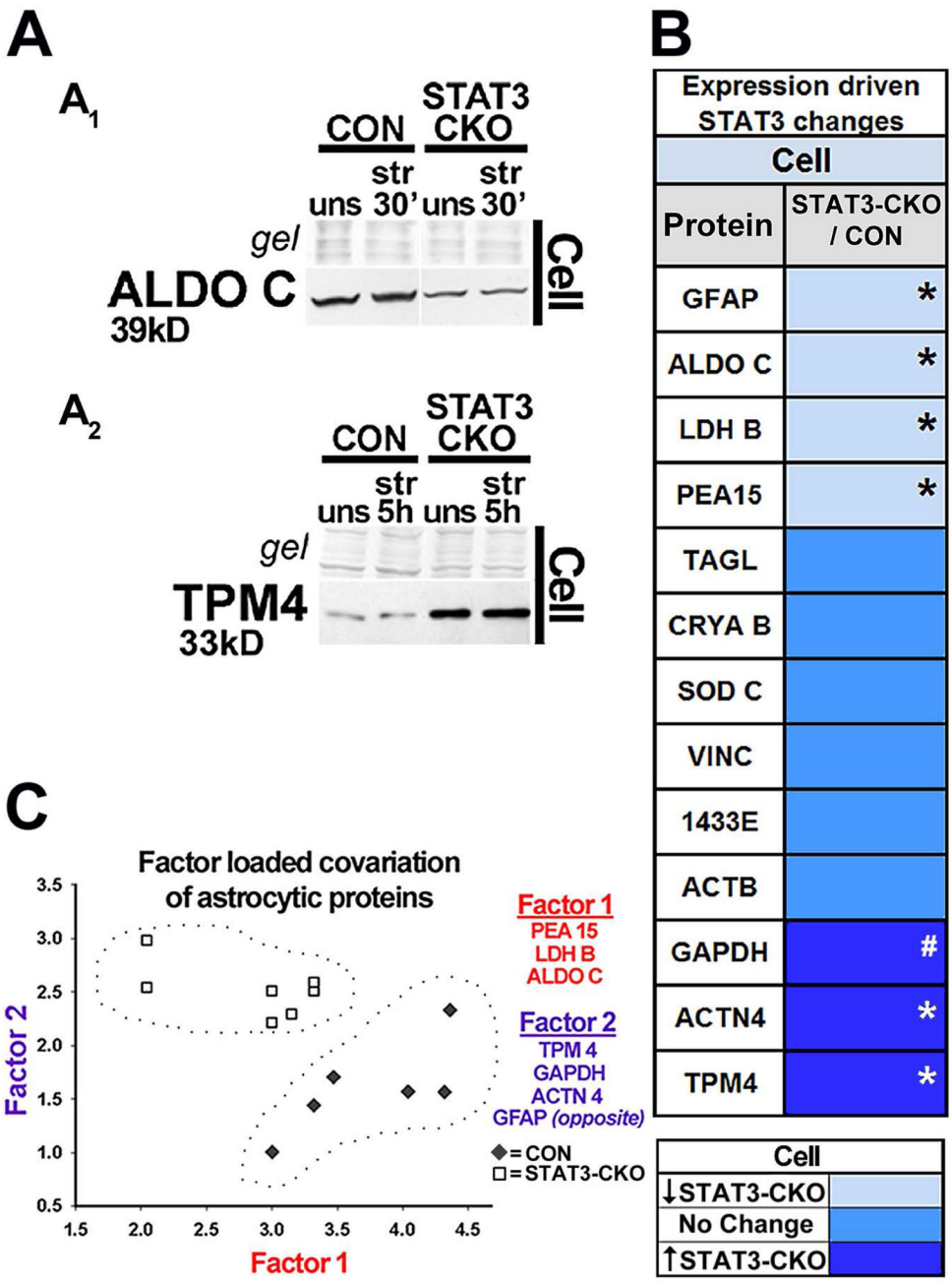

Figure 5. Identification of STAT3 regulated astrocytic proteins

A, Immunoblots show STAT3-CKO astrocyte cell lysates with reduced protein levels for ALDOC (***A_{1}***) and increased levels for tropomyosin 4, TPM4 (***A_{2}***) compared to CON astrocytes. ***B,*** Unstretched STAT3-CKO astrocytes had decreased average protein amounts compared to CON astrocytes (≤0.5, light blue) for ALDOC and GFAP (*p≤ 0.001, see A_1 and Fig. 7B), PEA15 (*p<0.01, Fig. 7A) and LDHB (*p≤ 0.05, shown in Fig. $4A_3$). Unstretched STAT3-CKO astrocytes had increased protein levels versus CON astrocytes (≥0.5, dark blue) for TPM4 and ACTN4 (*p<0.01, see A_2 and Fig. $4A_2$) and GAPDH (# p=0.07, shown in Fig. $4A_1$), as determined by repeated measurement ANOVA in n=5–8

mice from each genotype per protein. ***C,*** Biplot shows weighted mean protein amounts between paired CON (◆) and STAT3-CKO (□) unstretched cell samples based on Spearman Correlations between 13 astrocytic proteins. CON and STAT3-CKO protein levels are segregated by two underlying factors (encircled). PEA 15, LDHB, and ALDOC covaried by factor 1 (red). TPM4, GAPDH, ACTN4, and GFAP covaried by factor 2 (purple), with GFAP's loading in opposite direction (n=7 mice per genotype).

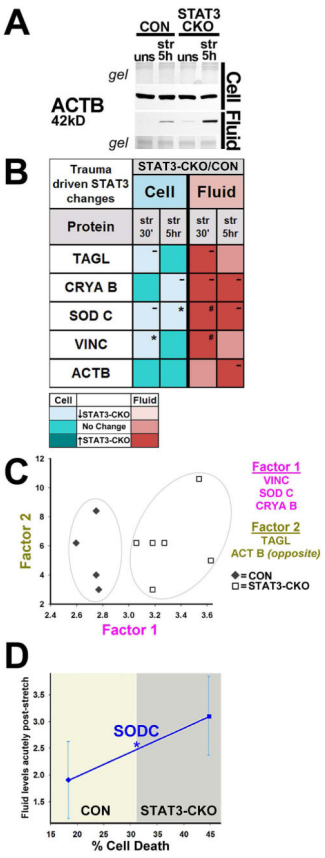

Figure 6. Elevated fluid proteins capture STAT3 deficient cell death increase

A, Immunoblot shows increased fluid levels of ACTB in STAT3-CKO versus CON by 5 h post-injury while cellular levels were similar. ***B,*** Mean cell (turquoise) and fluid (red) injury-induced protein changes between STAT3-CKO and CON astrocytes for 5 astrocytic proteins with same base expression in both genotypes (WCL n=3–5, CM n=2–5 animals per genotype and timepoint). STAT3-CKO had higher release than CON cultures at one or both timepoints post-injury (darker red boxes, # p=0.09 for SODC, # p=0.08 for VINC, both 30 min post-injury). STAT3-CKO had larger trauma-induced cellular losses versus CON astrocytes for TAGL, CRYAB, SODC and VINC (lighter turquoise; *p<0.05 for SODC at 5 h and for VINC at 30 min post-injury). ***C,*** Plotted are weighted mean fluid protein amounts at 30 min post-injury using Factor 1 (covariation of VINC, SODC and CRYAB) over Factor 2 (covariation between TAGL and ACTB) in stretched cultures of 4 CON and 6 STAT3-CKO animals. CON (◆) and STAT3-CKO (□) data are separated based on Factor 1 expressing a trauma response difference between genotypes (gray ellipses). ***D,*** Plotted is mean acute stretch-release of SODC (fluid change 30 min and 5 h after stretching) over percent delayed cell death (PI dye uptake at 48 h) in CON (◇) and STAT3-CKO (□) cultures (n=11 each genotype, * P=0.04, Mann-Whitney).

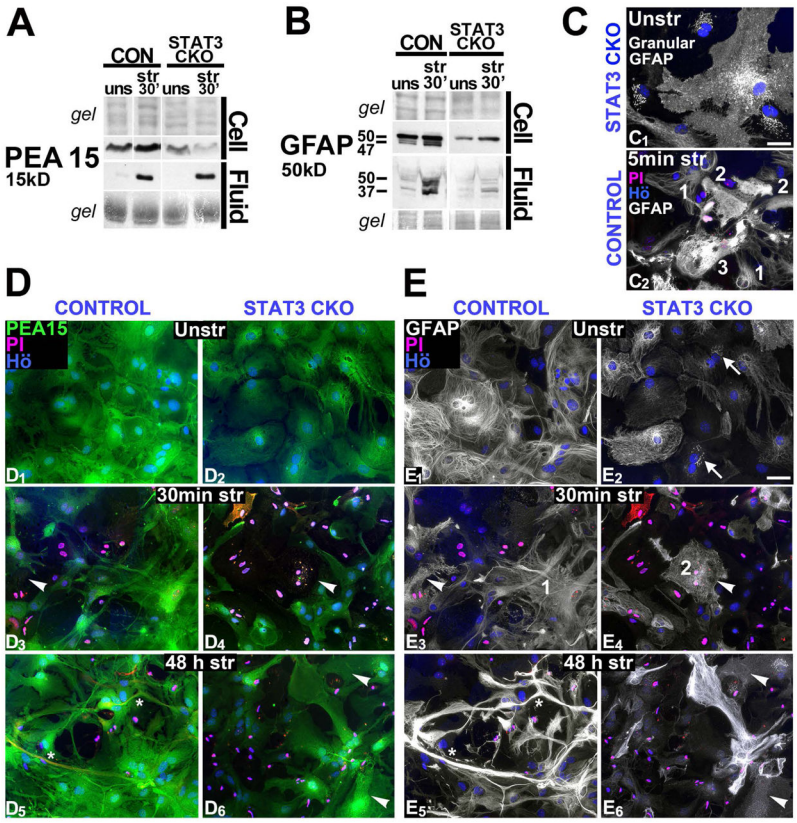

Figure 7. PEA15 and GFAP changes associate with astrocyte traumatic injury responses

A, Immunblots of PEA15 cell lysates were increased in CON cells at 30 min post-injury, and reduced in STAT3-CKO cells yet both genotypes similar PEA15 fluid signals at same post-injury time, despite lower STAT3-CKO versus CON base expression. ***B,*** Immunoblots show increased GFAP signals by 30 min post-injury in CON and STAT3-CKO astrocytes, who had overall attenuated GFAP amounts. GFAP was robustly elevated in fluids after stretching CON cultures but only marginally in STAT3-CKO cultures. Stretching increased a 47 kD cellular GFAP fragment and a 37 kD fluid GFAP fragment by 30 min post-injury. ***C,*** Immunofluorescence (IF) images show different subcellular GFAP distributions (white). ***(C_1)*** Unstretched STAT3-CKO astrocytes show granular GFAP aggregates around the nucleus stained by Hoechst dye (blue, see also arrows in E_2). ***(C_2)*** CON astrocytes at 5 min post-injury; **"1":** Filament-assembled GFAP, (also ***E_3*****). "2":** Filament-disassembled GFAP stain (see Methods) in stretch-injured cells with PI-positive (pink nuclei) permeable membranes (also ***E_4***). **"3":** PI-positive CON astrocytes show patches of brighter GFAP signals than surrounding GFAP staining. Scale bar = 20 μm. ***D+E,*** Set of IF images double-labeled for PEA15 (green***, D)*** and GFAP (white, ***E***) shows CON ***($D_{1,3,5}$; $E_{1,3,5}$)*** and STAT3-CKO ***($D_{2,4,6}$; $E_{2,4,6}$)*** astrocytes from unstretched ***($D_{1,2}$; $E_{1,2}$)*** and stretch-injured cultures at 30 min ***($D_{3,4}$; $E_{3,4}$)*** and 48 h ***($D_{5,6}$; $E_{5,6}$)*** post-injury. IF is combined with nuclear dye (Hoechst, blue) and unfixed PI uptake identifying permeable cells (red, pink nuclei). Arrowheads point at PEA15 depleted, permeable cells retaining disassembled GFAP. At 48 h post-injury CON cultures display reactive astrocytes with elongated processes and

elevated GFAP and PEA15 signals (asterisks) that are missing in STAT3-CKO cultures. Scale bar = 20 μm (D, E).

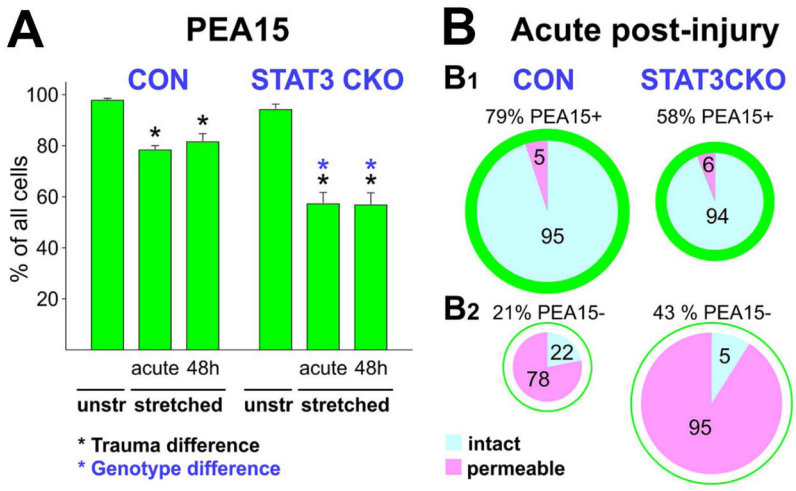

Figure 8. PEA15 depletion associates with astrocyte permeability after injury

A, Plotted are means and SEM of percent CON and STAT3-CKO astrocytes with PEA15 signals in unstretched and acutely stretched cultures (5 and 30 min post-injury combined) as well as 48 h post-injury. Black asterisks indicate significant loss of cells with PEA15 staining in stretched versus unstretched cultures ($P<0.05$). Genotype difference (blue asterisks) shows smaller PEA15-positive cell population in STAT3-CKO versus CON stretched cultures ($P<0.001$; post-hoc multiple comparison ANOVA Tukey, Table 4). ***B,*** Pie charts are sized to reflect proportions of PEA15-positive ***(B_{1})*** and PEA15–negative ***(B_{2})*** populations of all cells in both genotypes. Pies show fractions of permeable cells (PI-positive nuclei, pink) and non-permeable, intact cells (PI-negative nuclei, blue) acutely after stretching for both genotypes. The majority of PEA15-retaining cells were intact ***(B_{1})*** while PEA15 loss ***(B_{2})*** was strongly associated with cell permeability ($P<0.001$, Tukey-Kramer).

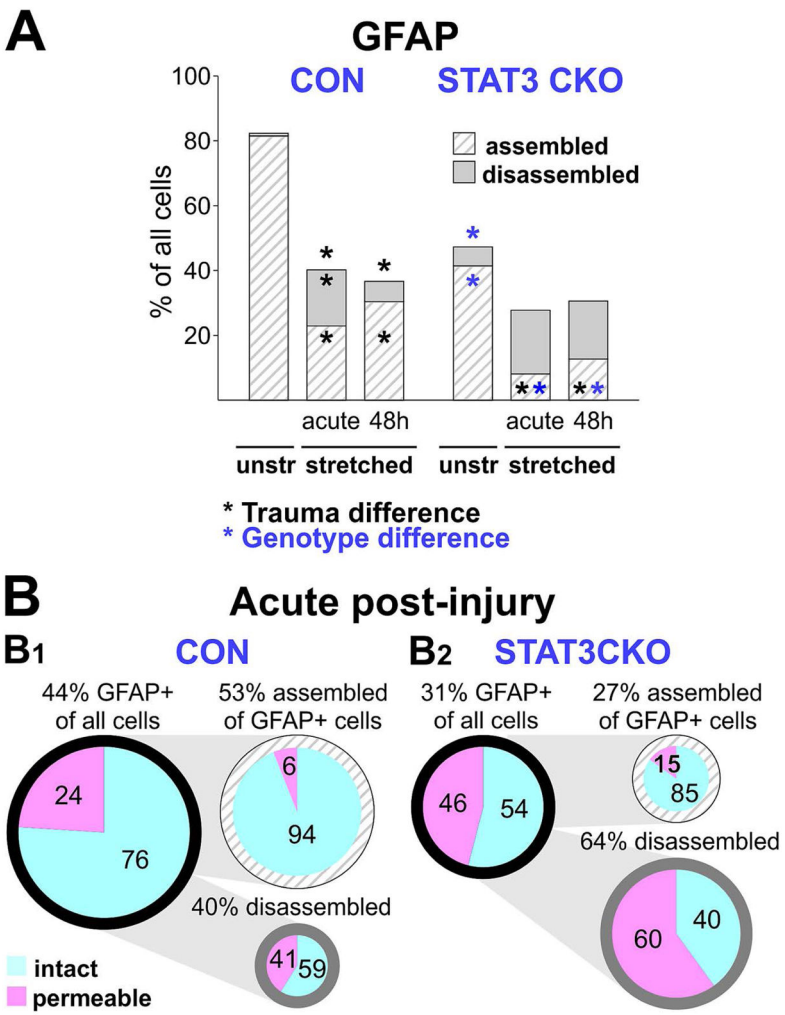

Figure 9. Loss in GFAP filament assembly and relation to astrocyte permeability after trauma

A, Stacked bars show average percent cells with GFAP and subpopulations with assembled (hatched) and disassembled (gray) GFAP in cultures of both genotypes unstretched, acute (5 and 30 min after stretching) and 48 h post-injury (SEMs see Table 5). There were fewer GFAP-positive cells in stretched versus unstretched CON astrocytes (black asterisks above CON bars, P<0.001, post-hoc multiple comparison ANOVA, Tukey). STAT3-CKO unstretched astrocytes had fewer GFAP-positive cells than CONs (P<0.01, blue asterisk above STAT3-CKO bar) and fewer cells with filament-assembled GFAP (blue asterisk in hatched bar, P<0,001). Percent astrocytes with filament-assembled GFAP decreased significantly versus unstretched cultures in both genotypes (black arrows on hatched bars, P<0.001). Filament-assembled astrocyte percentages declined further in STAT3-CKO versus CON stretched astrocytes (P<0.05, blue asterisks in hatched bars). ***B,*** Pie charts are sized to reflect the percent of GFAP-positive cells (black ring) and show the fractions of PI-permeable (pink) and intact cells (blue, PI-negative, non-permeable) acutely after stretching (5 min and 30 min data; means, SEMs and n, see Table 5). GFAP-positive CON astrocytes ***(B_1)*** had a smaller fraction of permeable cells than STAT3-CKO ones ***(B_2,*** P<0.05). Astrocytes with filament disassembled GFAP (gray pies) had significantly more permeable

cells than those with filament assembled GFAP (hatched pies) in both genotypes ($P<0.001$ for CON, $\boldsymbol{B_1}$; $P<0.01$ for STAT3-CKO GFAP subpopulations, $\boldsymbol{B_2}$). The small population of astrocytes with bright GFAP signals contributed to the GFAP-positive pool (data see Table 5).

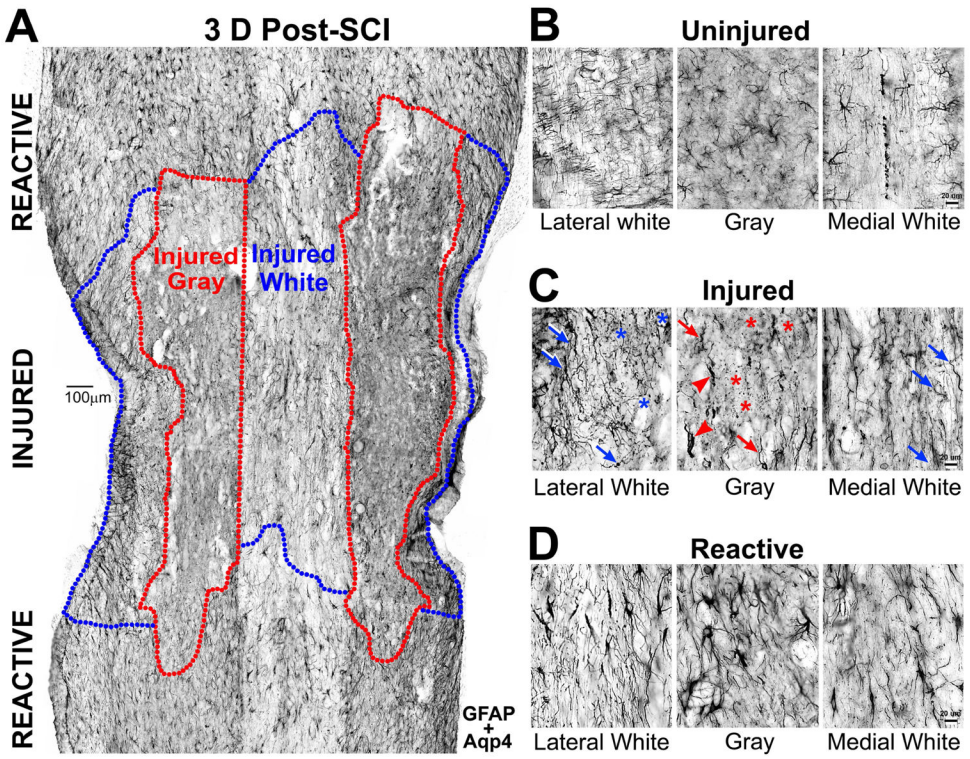

Figure 10. Injury and reactivity of gray and white matter astrocytes after spinal cord injury

A, Horizontal CON spinal cord section 3 days (D) after crush spinal cord injury (SCI) is stained for GFAP and aquaporin 4 (Aqp4). Gray (red) and white (blue) matter injury zones are delineated based on the presence of injured protoplasmic and fibrous astrocytes. Territorial reactive astrocytes populate caudal and rostral flanking penumbra areas. Scale bar = 100 μm. ***B,*** Images show uninjured astrocytes in lateral and medial white and gray matter sections with same stains as in A. They had thin processes and inconspicuous cell bodies. ***C,*** Shown are injured astrocytes in injury zones delineated in A. Asterisks label disintegrated astrocytes. Arrows point at tortuous and beaded astrocyte processes. Arrowheads show gray matter astrocytes with amputated processes. ***D,*** Images show reactive astrocytes far from the lesion in penumbra territories with enlarged cell bodies and thick processes. Bar for (B–D) = 20 μm.

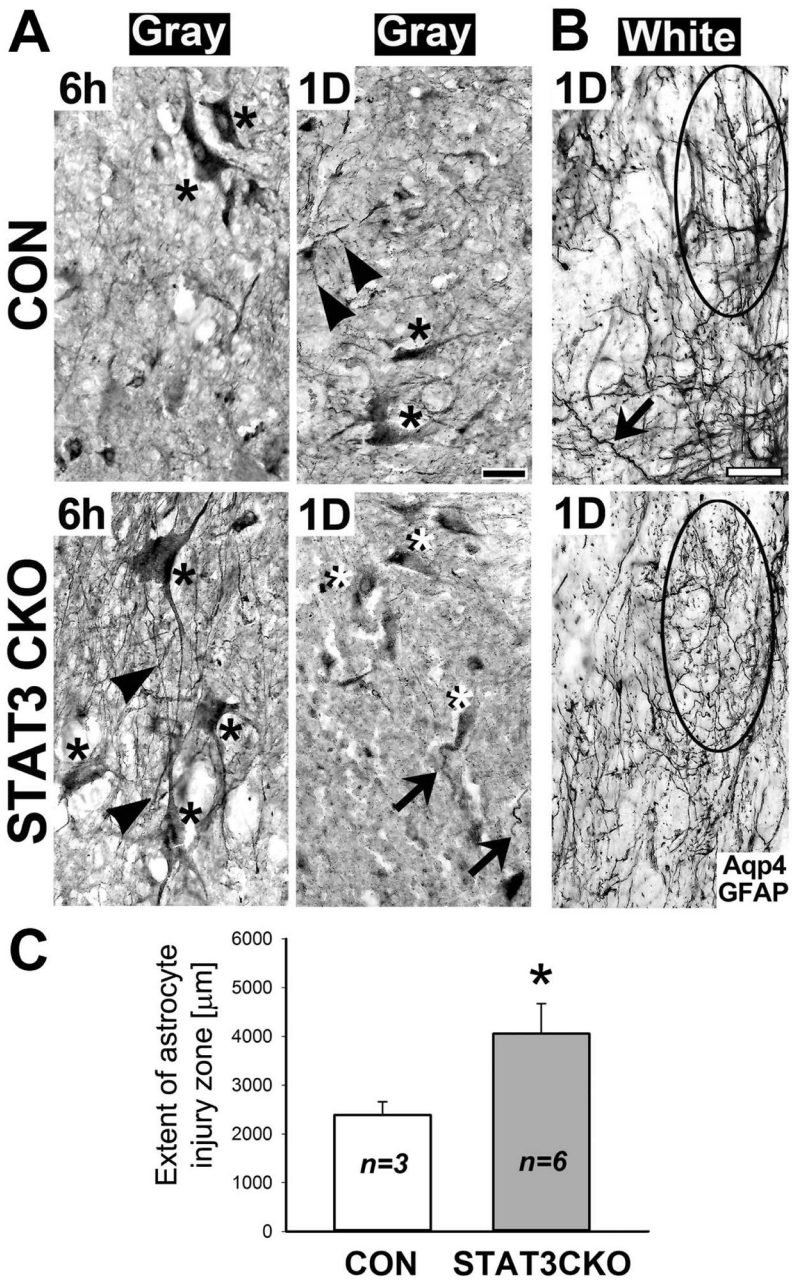

Figure 11. STAT3-CKO astrocytes show exacerbated acute injury in crush injured spinal cords

A, Aquaporin 4 (Aqp4) and GFAP stained gray matter tissue contains injured protoplasmic astrocytes with swollen cell bodies (asterisks) and thin processes (arrowheads) at 6 h after moderate crush SCI. Cell bodies of STAT3-CKO astrocytes were larger, more swollen, than those of CON astrocytes. By 1 day post-injury, protoplasmic CON astrocytes (black asterisk) retained processes (arrowheads), while STAT3-CKO cell bodies (white asterisks) had missing or truncated processes (arrows). Black bar = 20 μm. ***B,*** Astrocytes of injured white matter show process damage in CON (top) and STAT3-CKO (bottom) cords. STAT3-CKO fibrous astrocytes were more disintegrated than CON white matter, bearing tortuous, but continuous processes (arrow). Encircled are a reactive CON and injured STAT3-CKO

astrocytes. White bar = 20 μm. ***C,*** The extent of astrocyte injury zones is plotted for CON and STAT3-CKO white matter tissues within 1 day post-SCI. The distance from lesion center to territorial reactive astrocytes was measured (means and SD are given in μm, 5–9 sections were measured for each animal, n= 3–6 animals). Two-tailed T-test shows significantly larger extent of astroglial injury zones in STAT3-CKO versus CON cords (asterisk, $P<0.02$).

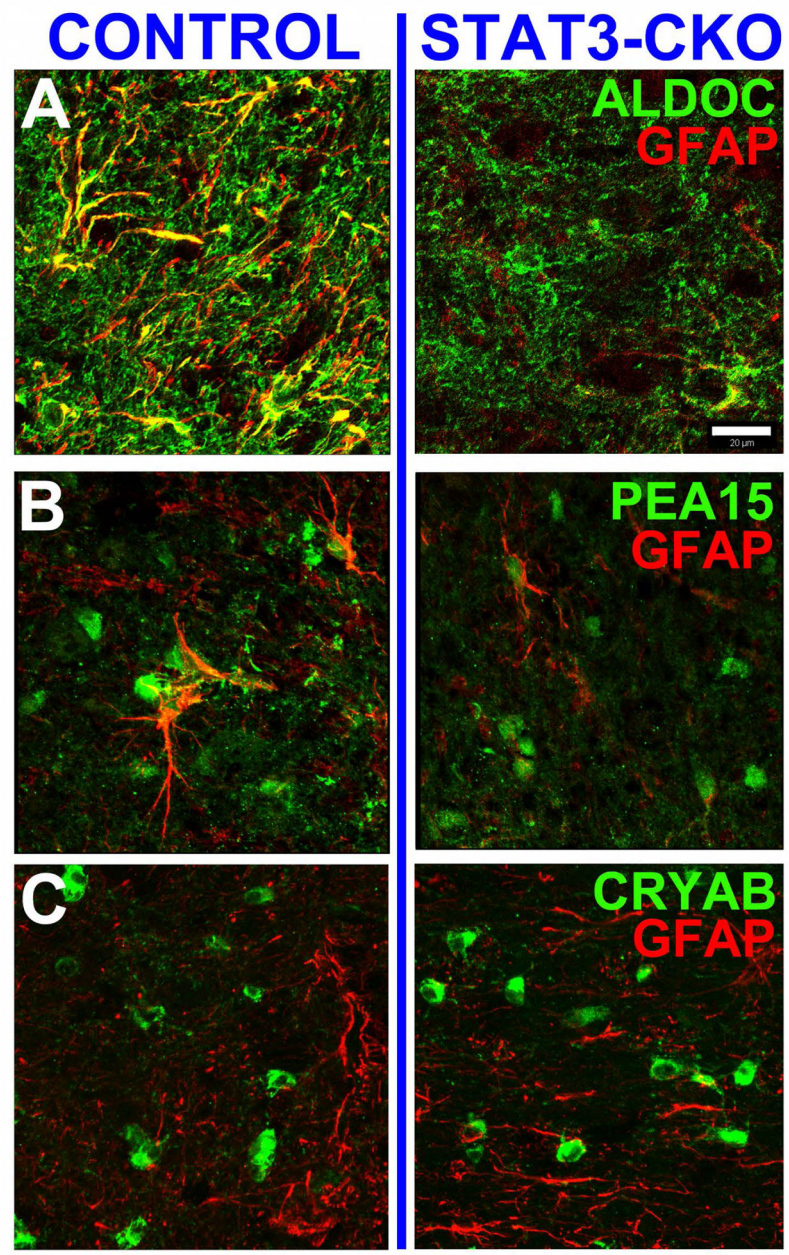

Figure 12. STAT3-dependent presence of Aldolase C and PEA15 in uninjured spinal cords and absence of α Crystallin

Shown are gray matter astrocytes of uninjured CON and STAT3-CKO spinal cords stained for GFAP (red) and in green (A) ALDOC, (B) PEA15 and (C) CRYAB. ***A,*** Left: ALDOC was strongly expressed in CON astrocytes, staining GFAP-positive processes (yellow) and fine process endings (green) that lacked GFAP. Right: GFAP and ALDOC signals were attenuated in STAT3-CKO astrocytes. ***B,*** PEA15 (green) was expressed in few CON astrocytes (left) and shows fainter signals in few STAT3-CKO astrocytes (right). ***C,*** GFAP-positive astroglial profiles (red) are shown without CRYAB signals, while other spinal neural cells expressed CRYAB irrespective of genotype (green). Bar = 20 μm.

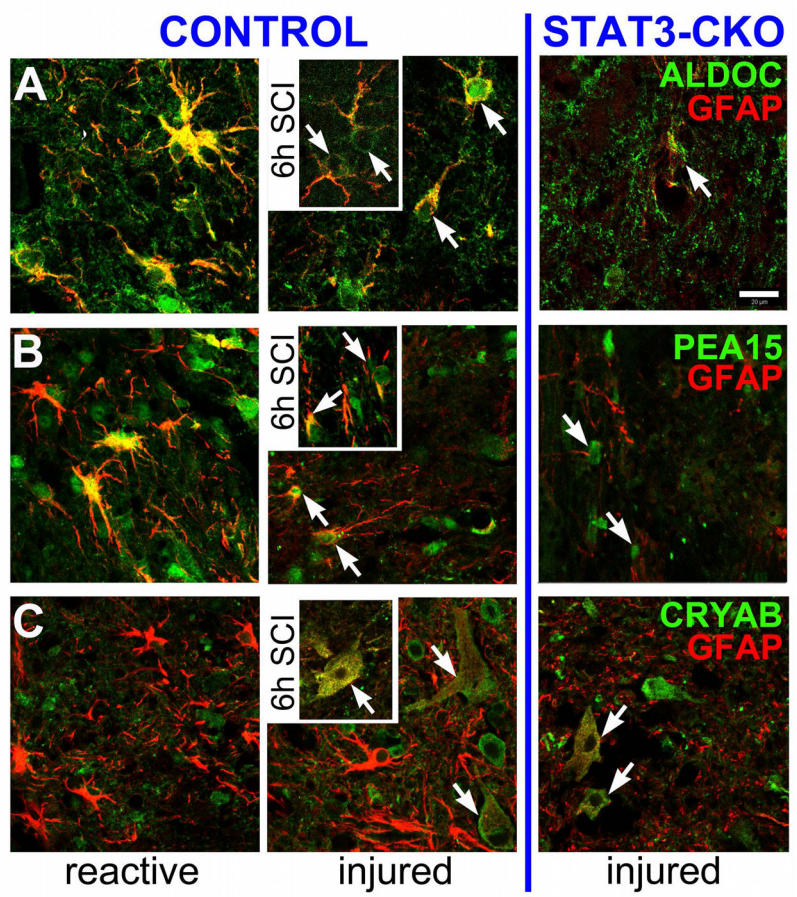

Figure 13. ALDOC, PEA15 and CRYAB distinguish reactive and injured astrocytes acutely after spinal cord crush injury

Shown are gray matter astrocytes one day (main) and 6 hr (inserts) post-SCI in Control (left) and STAT3-CKO (right) spinal cords. ***A,*** ALDOC and GFAP were robustly co-expressed in territorial, reactive astrocytes in the penumbra around the lesion (left). STAT3-CKO cords at same time post-SCI were missing reactive astrocytes (not shown). Areas near or within the lesion contained injured astrocytes showing ALDOC depletion (6h post-SCI, arrows) or attenuated signals (1d post-SCI, center, arrows). ALDOC and GFAP signals were faint in lesioned areas of STAT3-CKO astrocytes (right, arrow). ***B,*** At one day post-injury, reactive astrocytes co-expressed PEA15 and GFAP (yellow) in their cell bodies that were found in the lesion penumbra of CON cords (left). Injured CON spinal tissue had few PEA-15 expressing astrocytes with faint (1d post-SCI, center) to marginal (6 h, insert) PEA15 signals (green, arrows), while still showing GFAP (red, center and insert). Right: STAT3-CKO lesioned tissues had marginal astroglial PEA15 signals that was surrounded by faintly stained GFAP-positive processes (red, arrows). ***C,*** CRYAB was absent in strongly GFAP-positive reactive CON astrocytes (left, red), but was expressed in injured CON astrocytes with swollen cell bodies and thin processes where it was colocalized with weak GFAP signals (yellow, 6h insert, arrow). Similarly, injured STAT3-CKO astrocytes showing alike morphologies also expressed CRYAB colocalized with GFAP (right, arrows). Bar = 20 μm.

Table 1

List of primary antibodies for Western blotting, immunocytochemistry and immunohistochemistry

Primary antibodies	Company	Western blot dilution		Cell staining dilution	
Host, protein (SwissProt name)		**WCL**	**CM**	**In vitro**	**In vivo**
Rabbit anti-α-actinin (ACTN4)	Epitomics	1:20,000	1:2,000		
Rabbit anti-aquaporin 4(AQP4)	Sigma	N/A	N/A	N/A	1:10,000 (DAB)
Rabbit anti-Aldolase C (ALDOC)	GeneTex	1:20,000	1:3,000		
Goat anti-ALDOC	Santa Cruz				
Mouse IgG anti-αB-Crystallin (CRYAB)	Enzo Life Sciences	1:3,000	1:1,500		1:150 (IF)
Rabbit anti-apolipoprotein E (APOE)	Abcam	1:2,000	1:3,000		1:100 (IF)
Mouse IgG anti-β-actin (ACTB)	Sigma-Aldrich	1:70,000	1:3,000		
Mouse IgG anti-glyceraldehyde-3-phosphate dehydrogenase (GAPDH)	GeneTex	1:20,000	1:2000		
Rabbit anti-GFAP	Dako	1:500,000	1:10,000	1:600	1:20,000 (DAB)
Chicken anti-GFAP	Sigma-Aldrich	1:500,000	1:130,000		1:500 (IF)
Rabbit anti-glutamine synthetase (GLNA)*	Abcam	1:40,000	1:8,000		1:500 (IF)
Rabbit anti-lactate dehydrogenase (LDHB)	Cell Signaling	1:6,000	1:2,000		
Rabbit anti-PEA15	GeneTex	1:10,000	1:1,000	1:200	1:200 (IF)
Rabbit anti-peroxiredoxin (PRDX1)	Enzo Life Sciences	1:10,000	1:2,000		
Rabbit anti-superoxide dismutase (SODC)	Cell Signaling	1:7,000	N/A		1:100 (IF)
Rabbit anti-STAT3	GeneTex	1:200,000	1:10,000		
Rabbit anti-transgelin (TAGL)					
Rabbit anti-tropomyosin 4 (TPM4)	GeneTex	1:8,000	1:2,000		
Mouse IgM anti-vimentin (VIME)	Sigma-Aldrich	1:15,000	1:1,000		
Mouse IgG anti-vinculin (VINC)	Sigma-Aldrich	1:20,000	1:50,000		
Rabbit anti-Y wha 14-3-3-ε (1433E)	Chemicon	1:10,000	1:6,000		

*Femto ECL chemiluminescence substrate was used for the detection of GLNA enabling higher antibody dilution to suppress background.

Pico ECL was used for all other antibodies.

Table 2

List of secondary antibodies

Secondary antibodies	Company	Dilution**
Host, species reactivity, conjugation		
Western blotting:		
Goat anti-rabbit IgG, HRP conjugate	Thermo Scientific	1:10,000
Goat anti-mouse IgG, HRP conjugate	Thermo Scientific	1:10,000
Goat anti-mouse IgM, HRP conjugate	Thermo Scientific	1:7,500
Cell staining:		
Goat anti-rabbit biotinylated	Vector	1:200
Donkey anti-rabbit Alexa 488	Jackson ImmunoResearch	1:150
Donkey anti-chicken Cy3	Jackson ImmunoResearch	1:200
Donkey anti-mouse IgG Cy3	Jackson ImmunoResearch	1:200
Donkey anti-goat Alexa 488	Jackson ImmunoResearch	1:100

** Glycerol was added to a final conc. of 50 % to all secondary antibodies in recommended volume.

HRP: horseradish peroxidase

Fluorescent dyes: green: Alexa 488, orange: Cy3 and ‘far red’: Alexa 647

Table 3

Mouse proteomic trauma release list

Given are average fold protein changes in fluid (= conditioned medium, CM) due to mechanical injury of murine astrocytes using densitometric Sypro ruby spot measurements (triplicate gels for each CM sample from unstretched and stretched culture pairs of 6 CON and 4 STAT3-CKO mice). Listed are Swiss Prot IDs with significant changes 30 min and 5 h post-injury in each genotype (≥1.8 fold increase or ≤0.6 fold decrease of stretched over unstretched CM spot densities; P≤0.05, false discovery rate, see Methods). GFAP and SPARC were identified in addition to the listed proteins, but could not be reliably quantitated as multiple proteins were located on their spots. GFAP was confirmed by immunoblotting and IF (see Figs. 4, 5, 7 and 9–14).

			Average fold fluid change (str/unstr)			
Protein Name	**Swiss Protein**	**Unique Peptides**	**30 min**		**5 h**	
INCREASED			**CON**	**STAT3-CKO**	**CON**	**STAT3-CKO**
Actin, cytoplasmic 1 (Beta-actin)	*ACTB*	5	1.5	**1.9**	1.2	1.6
Alpha-actinin-4	*ACTN4*	27	1.1	**2.0**	1.4	1.4
Aldoa Fructose-bisphosphate aldolase A	*ALDOA*	13	**2.8**	**3.3**	**2.5**	**2.4**
Aldoc Fructose-bisphosphate aldolase C	*ALDOC*	20	**2.4**	**2.0**	1.6	1.6
Akr1b3 Aldose reductase	*ALDR*	8	**3.8**	**2.7**	1.7	**4.9**
Ass1 Argininosuccinate synthase	*ASSY*	11	1.7	**2.4**	**2.0**	**2.2**
Complement factor B precursor	*CFAB*	5	1.3	**2.1**	1.5	**1.9**
Clusterin	*CLUS*	5	1.1	**3.4**	0.8	**1.9**
Cofilin-1	*COF1*	7	**3.0**	**2.4**	**3.1**	**2.4**
Coactosin-like protein	*COTL1*	2	1.6	**2.2**	1.7	1.7
Alpha crystallin B chain	*CRYAB*	6	1.7	**3.1**	**2.9**	1.6
N(G), N(G)-dimethylarginine dimethylaminohydrolase 1	*DDAH1*	9	**2.5**	**2.9**	**3.0**	**5.1**
Dihydropyrimidinase-related protein 2	*DPYL2*	13	---	---	1.4	**1.9**
Elongation factor 2	*EF2*	11	---	---		**4.0**
Transcription elongation factor b polypepetide 2	*ELOB*	7	**1.8**	**2.3**	**1.8**	1.1
Alpha enolase	*ENOA*	28	**2.0**	**3.1**	1.4	**1.9**
S-formylglutathione hydrolase	*ESTD*	7	**2.4**	**4.0**	1.4	**3.6**
Fatty acid-binding protein, brain	*FABPB*	2	1.3	**2.1**	1.5	**1.9**
F-box only protein 2	*FBX2*	2	1.1	**3.4**	0.8	**1.9**
Filamin-A (Alpha-filamin)	*FLNA*	3	1.3	**2.1**	1.5	**1.9**
Glyceraldehyde-3-phosphate dehydrogenase	*GAPDH*	7	**6.4**	**5.6**	**4.6**	**5.4**

Protein Name	Swiss Protein	Unique Peptides	Average fold fluid change (str/unstr)			
			30 min		5 h	
INCREASED			**CON**	**STAT3-CKO**	**CON**	**STAT3-CKO**
G protein Beta 1, 2 subunit	*GBB1/2*	5	1.6	1.5	**1.8**	1.2
Glutamine Synthetase	*GLNA*	6	**2.7**	1.5	**1.9**	**2.9**
Glutamine oxaloacetate transaminase 1	*GOT1*	6	**2.4**	**2.0**	1.6	1.6
78kDa glucose-regulated protein	*GRP78*	3	1.3	**2.5**	1.7	**2.4**
Heat shock cognate 71kDa protein	*HSP7C*	25	1.3	**2.5**	1.7	**2.4**
Isocitrate dehydorgenase cytoplasmic	*IDHC*	15	**3.3**	**2.7**	**2.2**	**3.1**
Creatine kinase B-type	*KCRB*	16	1.6	**2.3**	1.6	1.5
L-lactate dehydrogenase B chain	*LDHB*	15	**1.9**	1.3	**2.0**	**2.8**
Malate dehydrogenase, cytoplasmic	*MDHC*	10	**2.4**	**2.6**	**2.4**	**2.7**
Nucleoside diphosphate kinase B	*NDKB*	7	**1.9**	1.7	**2.7**	**2.0**
Isoform of Obg-like ATPase 1	*OLA1*	3	1.7	**2.4**	**2.0**	**2.2**
Astrocytic phosphoprotein, 15kDa	*PEA15*	8	**1.9**	**2.3**	1.7	1.6
Phosphatidylethanolamine-binding protein 1	*PEBP1*	2	**3.7**	**3.3**	1.5	**2.3**
Phosphoglycerate kinase 1	*PGK1*	14	**3.0**	**3.0**	**2.7**	**3.1**
Peptidyl-prolyl cis trans isomerase A	*PPIA*	3	**1.9**	1.7	**2.7**	**2.1**
Peroxiredoxin-1	*PRDX1*	16	1.6	**2.1**	1.6	1.1
Peroxiredoxin-2	*PRDX2*	4	**3.7**	**3.3**	1.5	**2.3**
Secernin-1-Mus	*SCRN1*	7	1.4	**2.1**	1.0	1.3
Superoxide dismutase [Cu-Zn]	*SODC*	5	**2.4**	**3.5**	**3.1**	**3.9**
Transgelin (Smooth muscle protein 22-alpha)	*TAGL*	7	1.6	**2.1**	1.6	1.1
Transitional ER ATPase	*TERA*	26	**2.1**	**4.0**	**2.7**	**3.4**
Tropomyosin alpha-1 chain	*TPM1*	19	1.5	**2.0**	1.3	1.7
Tropomyosin alpha-3,4 chain	*TPM3/4*	20	**2.1**	**2.0**	1.2	1.2
Vinculin	*VINC*	30	1.0	**1.9**	1.2	1.2
Ywhae 14-3-3 protein epsilon, zeta/delta	*1433E/Z*	20	**1.9**	**2.0**	1.4	**1.9**
Ywhae 14-3-3 protein B, F, G, T	*1433B/F/G/T*	15	1.4	**1.9**	1.0	1.5
DECREASED						
Apolipoprotein E	*APOE*	12	0.8	**0.5**	0.7	**0.3**

Protein Name	Swiss Protein	Unique Peptides	Average fold fluid change (str/unstr)			
			30 min		5 h	
INCREASED			**CON**	**STAT3-CKO**	**CON**	**STAT3-CKO**
Gelsolin	*GELS*	8	0.8	**0.6**	1.2	1.1
Haptoglobin	*HPT*	5	0.8	1.1	**0.6**	0.9
Inter-alpha-trypsin inhibitor (heavy chain)	*ITIH2*	3	0.8	**0.6**	0.8	**0.6**
Plastin-2	*PLSL*	4	---	---	0.9	**0.1**
Serine/Threonine Protein phosphatase 2A	*2AAA*	8	0.8	1.0	0.8	**0.6**

Table 4

PEA15 population and permeability quantitation

Given are mean and SEM of percent PEA15-positive (PEA15+, green) and PEA15-negative (PEA15−, white) CON and STAT3-CKO astrocytes for unstretched (n=5 mice of each genotype), acute post-injury (combining same trend 5 min and 30 min post-injury data, n=10 CON and 5 STAT3-CKO mice) and 48 h post-injury cultures (n=5 mice of each genotype). Percent membrane permeable cells were determined of all cells and for PEA15-positive and −negative fractions (PI-positive, PI+ pink columns).

		%	PEA15+		PEA15-	
Genotype	**Time post-injury**	**PI+**		**PI+ of PEA15+**		**PI+ of PEA15-**
CON	unstr	N/A	98 ± 1	N/A	2 ± 1	N/A
	acute	22 ± 7	79 ± 5	5 ± 3	21 ± 5	78 ± 12
	48 h	16 ± 9	83 ± 6	3 ± 2	17 ± 6	73 ± 26
STAT3 CKO	unstr	N/A	95 ± 5	N/A	5 ± 5	N/A
	acute	44 ± 11	58 ± 9	6 ± 2	43 ± 9	91 ± 11
	48h	53 ± 6	52 ± 9	12 ± 3	48 ± 9	98 ± 1

Table 5

Quantification of subcellular GFAP distribution patterns and cell permeability

Listed are mean percentages +/− SEM of GFAP-positive populations (GFAP+, black column) that were comprised of filament assembled (hatched) and disassembled (gray) signals and a small population of cells with far above average bright GFAP signals (yellow column). STAT3-CKO astrocytes had a considerable cell fraction with granular GFAP aggregates (light gray column). Populations were analyzed in cultures that were unstretched (n=5 mice each genotype), acutely stretched (5 and 30 min post-injury combined, n=10 CON and 5 STAT3-CKO mice) and at 48 h post-injury (n=5 mice each genotype).

		%	GFAP+		Assembled GFAP		Disassembled GFAP		Bright GFAP		Granular GFAP	
Genotype	Time post-injury	PI+	of all	PI+ of GFAP+	of GFAP+	PI+ of assembled	of GFAP+	PI+ of Dis-assembled	of GFAP+	PI+ of Bright	of all	PI+ of Granular
CON	unstr	N/A	83 ± 2	N/A	99 ± 29	N/A	1 ± 6	N/A	0 ± 0	N/A	1 ± 1	N/A
	acute	22 ± 7	44 ± 9	24 ± 14	53 ± 18	6 ± 5	40 ± 17	41 ± 16	7 ± 2	68 ± 14	1 ± 1	59 ± 38
	48 h	16 ± 9	38 ± 6	12 ± 12	80 ± 17	4 ± 1	16 ± 14	39 ± 10	3 ± 4	78 ± 42	1 ±1	5 ± 14
STAT3 CKO	unstr	N/A	48 ± 3	N/A	87 ± 7	N/A	12 ± 3	N/A	0 ± 0	N/A	18 ± 12	N/A
	acute	44 ±10	31 ± 10	46 ± 12	27 ± 13	15 ± 14	64 ± 10	60 ± 15	9 ± 5	59 ± 28	10 ± 8	44 ± 27
	48 h	53 ± 6	35 ± 16	41 ± 11	37 ± 14	10 ± 5	51 ± 13	56 ± 6	12 ± 4	66 ± 24	9 ± 7	32 ± 8